Title: β2-microglobulin triggers NLRP3 inflammasome activation in tumor-associated macrophages to promote multiple myeloma progression.

Authors: Daniel Hofbauer[1*], Dimitrios Mougiakakos[1*], Luca Broggini[2, 11], Mario Zaiss[3], Maike Büttner-Herold[4], Christian Bach[1], Bernd Spriewald[1], Frank Neumann[5], Savita Bisht[6], Jens Nolting[6], Robert Zeiser[7], Shaima'a Hamarsheh[7], Martin Eberhardt[8], Julio Vera[8], Cristina Visentin[2], Chiara Maria Giulia De Luca[9], Fabio Moda[9], Stefan Haskamp[10], Cindy Flamann[1], Martin Böttcher[1], Katrin Bitterer[1], Simon Völkl[1], Andreas Mackensen[1], Stefano Ricagno[2], and Heiko Bruns[1, 12]

Affiliations: [1]Department of Internal Medicine 5, University Hospital Erlangen, Erlangen, GER; [2]Department of Bioscience, University of Milan, Milan, ITA; [3]Department of Internal Medicine 3, University Hospital Erlangen, Erlangen, GER; [4]Department of Nephropathology, University Hospital Erlangen, Erlangen, GER; [5]Department of Internal Medicine 1, Saarland University Medical School, Homburg, GER; [6]Department of Oncology/Hematology and Rheumatology, University Hospital Bonn, Bonn, GER; [7]Department of Medicine 1, University of Freiburg, Freiburg, GER; [8]Department of Dermatology, University Hospital Erlangen, Erlangen, GER; [9]Divisione di Neurologia 5 - Neuropatologia, Fondazione IRCCS Istituto Neurologico Carlo Besta, Milano, Italy. [10]Institute of Human Genetics, Universitätsklinikum Erlangen, Friedrich-Alexander-Universität Erlangen-Nürnberg, Erlangen 91054, Germany, [11]Institute of Molecular and Translational Cardiology, IRCCS Policlinico San Donato, San Donato Milanese, Milano, Italy.
[12]Lead contact

* These authors contributed equally.

Correspondence: Heiko Bruns, Department of Internal Medicine 5 - Hematology/Oncology, FAU, Erlangen, Germany, Ulmenweg 18, D-91054 Erlangen. Phone: +49 09131-85-43163, Fax: +49-9131-85-36521, E-Mail: heiko.bruns@uk-erlangen.de

Summary

As substantial constituents of the multiple myeloma (MM) microenvironment, pro-inflammatory macrophages have emerged as key promoters of disease progression, bone destruction, and immune-impairment. We identified beta-2-microglobulin (β2m) as a driver in initiating inflammation in myeloma-associated macrophages (MAMs). Lysosomal accumulation of phagocytosed β2m promoted β2m amyloid aggregation in MAMs, resulting in lysosomal rupture, and ultimately in production of active interleukin (IL)-1β and IL-18. This process depended on activation of the NLRP3 inflammasome after β2m accumulation, as macrophages from NLRP3-deficient mice lacked efficient β2m-induced IL-1β production. Moreover, depletion or silencing of β2m in MM cells abrogated inflammasome activation in a murine MM model. Finally, we demonstrated that disruption of NLRP3 or IL-18 diminished tumor growth and osteolytic bone destruction normally promoted by β2m-induced inflammasome signaling. Our results provide mechanistic evidence for β2m's role as an NLRP3 inflammasome activator during MM pathogenesis. Moreover, inhibition of NLRP3 represents a potential therapeutic approach in MM.

Introduction

Multiple myeloma (MM) is an incurable B-cell malignancy characterized by accumulation of malignant plasma cells in the bone marrow (BM) (Palumbo and Anderson, 2011), lytic bone lesions (Terpos et al., 2013) and the ability to manipulate the BM environment (Kawano et al., 2015; Rutella and Locatelli, 2012). It is widely accepted that dysregulated inflammatory and immunological processes in the tumor microenvironment are not mere bystander effects but that invading leucocytes and tumor-associated macrophages (TAMs) are central for the initiation and progression of MM (Coussens and Werb, 2002; Hebron et al., 2013; Prabhala et al., 2010; Roussou et al., 2009). Studies have suggested that TAMs in MM support proliferation (Kim et al., 2012) and drug resistance (Zheng et al., 2009) of MM cells, and that high TAM content correlates with poor prognosis (Suyani et al., 2013). TAMs acquire a strongly pro-inflammatory transcriptional profile in the MM microenvironment (Kim et al., 2012) and produce pro-inflammatory cytokines including interleukin-6 (IL-6) (Durie et al., 1990), IL-1β (Hope et al., 2014), and tumor necrosis factor (TNF) (Hideshima et al., 2001), which in turn favor MM progression and severity (Hope et al., 2014). More recently, abundance of the pro-inflammatory IL-18 has been identified as a key promoter of MM (Nakamura et al., 2018). Moreover, systemic inhibition of inflammation (Alexanian et al., 1986; Richardson et al., 2003) or targeting of IL-1β prolongs progression-free survival of MM patients and delays disease onset (Lust et al., 2009), which indicates that interfering with inflammatory pathways, may potentially hold great therapeutic promise. Despite the central function attributed to TAMs in promoting MM, the initiating pathways that ultimately lead to the pro-inflammatory activation of macrophages remain completely unclear.

Because of their highly inflammatory nature, IL-1β and IL-18 production is tightly controlled by cytosolic multiprotein complexes known as “inflammasomes”. One of the most widely studied inflammasome complexes is nod-like receptor family pyrin domain-containing 3 (NLRP3), which has been implicated in a wide range of diseases, including Alzheimer’s

disease (Halle et al., 2008), gout (Martinon et al., 2006), type 2 diabetes (Masters et al., 2010), infectious diseases (Lightfield et al., 2008) (Rathinam et al., 2010), and cancer (Hamarsheh and Zeiser, 2020). After being activated, NLRP3 recruits the adaptor molecule ASC, which in turn binds to procaspase-1, leading to its autocatalytic processing and activation. Active caspase-1 catalyzes cleavage of the pro-cytokines IL-1β and IL-18, which are secreted and biologically active only in their processed forms (Latz et al., 2013). Signals and mechanisms leading to inflammasome activation are still poorly understood. The NLRP3 inflammasome can be activated by microbial cell wall components and toxins (Sutterwala et al., 2007). However, the inflammasome is also proficient in sensing stress or endogenous danger signals, such as extracellular ATP (Mariathasan et al., 2006), crystalline substances (Hornung et al., 2008) or amyloid β fibrils (Halle et al., 2008). The latter initiated NLRP3 activation by perturbation of cytoplasmic homeostasis due to lysosomal destabilization (He et al., 2016). This process, triggered by phagocytosed aggregated or insoluble materials, is characterized by the cytosolic release of lysosomal contents (like cathepsins) and reactive oxygen species (ROS), which results in assembly of the NLRP3 inflammasome and activation of caspase-1. Despite the key role of inflammation in MM progression, little is known about the relevance and initiating pathways of inflammasome activation in MM.

β2-microglobulin (β2m) is a non-glycosylated protein composed of 119 amino acid residues with a secreted form of 99 amino acids and a molecular mass of 11,800 Dalton. β2m is synthesized by all nucleated cells and forms complexes with the heavy chain of major histocompatibility complex (MHC) class I antigen through noncovalent linkage on cell surfaces (Bjorkman et al., 1987) (Halabelian et al., 2014). While under physiological conditions, β2m is generated at a constant rate, elevated β2m serum concentrations are observed in a range of autoimmune, renal, and hematological diseases. In particular wild type and the D76N β2m variants are responsible of two amyloid related diseases indicating a clear amyloid aggregation propensity for monomeric β2m *in vivo* (Gejyo et al., 1985) (Valleix et

al., 2012). In MM, increased β2m concentrations are correlated with a poor prognosis (Greipp et al., 2005) (Palumbo et al., 2015) and the failure of MM patients to respond to therapy (Bataille et al., 1984). Although the biological effects of β2m in MM remains enigmatic, earlier studies have reported β2m uptake by myeloid cells and an induction of a pro-inflammatory immune response (Miyata et al., 1994).

Here, we found that the NLRP3 inflammasome is activated after phagocytosis of β2m and that internalized β2m aggregates into amyloid fibrils under the acidic phagosomal conditions, which results in lysosomal swelling and damage. We further demonstrated that the β2m-triggered NLRP3 activation in TAMs resulted in the release IL-1β and IL-18 and, in turn favored the growth and severity of MM. Our findings provide insights into the molecular processes underlying the inflammatory conditions of MM and indicate that β2m represents an inducer of sterile inflammation in macrophages.

Results

β2m induces IL-1β and IL-18 release by macrophages in a caspase-1 and NLRP3-dependent manner. It remains unexplained how the inflammatory microenvironment in MM is initiated. Given the fact that β2m concentrations increase during MM progression, as well as the finding that ingested β2m triggers a pro-inflammatory immune response, we hypothesized that β2m induces inflammasome activation in macrophages. Initially, we investigated whether β2m treatment promotes release of IL-1β and IL-18 by human macrophages. Given that pro-IL-1β is not constitutively expressed and requires transcriptional induction, we primed cells with lipopolysaccharide (LPS), to ensure robust induction of pro-IL-1β and to mimic the chronic activation of macrophages in inflammatory diseases. We found that β2m induced a dose-dependent release of IL-1β and IL-18 in comparison to controls (**Fig. 1A**), whereas protease digested β2m had no effect (**Supplementary Fig. 1A**). In addition, IL-1β and IL-18 secretion was inhibited in the presence of an anti-β2m blocking

antibody but not by control IgG (**Supplementary Fig. 1A**), indicating that β2m is the active soluble factor responsible for the release of IL-1β and IL-18.

To confirm the β2m-triggered inflammasome activation in macrophages, we performed immunoblot analysis of cell lysates and supernatants (**Fig. 1B**). Firstly, we observed high expression of NLRP3 and the concomitant adaptor oligomer ASC in cell lysates of β2m- and nigericin-treated macrophages. In addition, we monitored low basal intracellular protein concentrations of further inflammasome markers, such as pro-IL-1β (p31) and pro-caspase-1 (p45). Detection of active caspase-1 (p20) in cell supernatants revealed that β2m induced specific cleavage of caspase-1 to its functional subunits p10 and p20, which appeared to be partially released. As expected, intracellularly processed cytokines IL-1β (p17) and IL-18 (p22) were detected in cell supernatants of β2m- and nigericin-treated macrophages (**Fig. 1B**). To test whether β2m activates caspase-1, we measured caspase-1 activation in β2m-treated macrophages using FLICA® reagent, a cell-permeant fluorescent-labeled inhibitor specifically binding to active caspase-1 (**Fig. 1C**). Confocal microscopy as well as flow cytometry showed an increase in caspase-1-positive macrophages after treatment with β2m (**Fig. 1C**, right). The β2m-triggered increase in caspase-1-positive macrophages was similar to the positive control nigericin (**Fig. 1C**, middle**; Supplementary Fig. 1B**). In contrast, macrophages treated with $\beta2m_{digest}$ or β2m in presence of a neutralizing antibody (αβ2m) showed no activation (**Supplementary Fig. 1C**). We found no ("off-target") effects of the αβ2m antibody on nigericin-mediated IL-1β and IL-18 release or caspase-1 activation (**Supplementary Fig. 1D**). To verify the observed impact of β2m on caspase-1 activation, we treated macrophages with β2m in presence of a caspase-1-specific inhibitor z-YVAD-fmk and measured IL-1β in supernatants by ELISA. We noted nearly complete inhibition of IL-1β release by macrophages (**Fig. 1D**), indicating that β2m-induced release of IL-1β is mediated by activated caspase-1. Next, we investigated whether the inflammasome adaptor oligomer ASC might be present in macrophages, since it is required for autocatalysis of pro-caspase-1 converting into

active caspase-1 (**Fig. 1E**). We therefore analyzed ASC oligomerization in β2m- and nigericin-treated macrophages. Confocal microscopy revealed an increase in ASC oligomerization after β2m treatment (**Fig. 1E** and **Fig. 1F**), similar to the NLRP3-dependent control nigericin (**Fig. 1E** and **Fig. 1F**). Finally, we examined whether β2m specifically induces NLRP3 inflammasome activation. Therefore, we treated LPS-primed BM cells from wild-type (C57BL/6, WT) and NLRP3-deficient (*Nlrp3*$^{-/-}$) mice with β2m as well as with NLRP3-dependent (ATP, nigericin) and NLRP3-independent (poly(dA:dT) (poly(deoxyadenylic-thymidylic) acid)) stimuli (**Fig. 1G** and **Supplementary Fig. 1E**). Increasing the amount of β2m, we detected a dose-dependent induction of IL-1β and IL-18 secretion by BM cells from wild-type mice, as well as observed for NLRP3-independent control poly(dA:dT). In contrast, we found that IL-1β and IL-18 release by BM cells from *Nlrp3*$^{-/-}$ mice was nearly abolished after β2m treatment, as well as observed for NLRP3-dependent controls (ATP, nigericin) (**Fig. 1G** and **Supplementary Fig. 1E**). To confirm that β2m specifically triggers NLRP3 inflammasome activation, we treated macrophages with β2m in the presence of the NLRP3-specific inhibitor MCC950 (Coll et al., 2015). Treating macrophages with nanomolar concentrations of MCC950 inhibited the β2m-triggered release of IL-1β (**Fig. 1H**). These data collectively indicate that β2m induces the release of IL-1β and IL-18 from macrophages in a caspase-1 and NLRP3-dependent manner.

Phagocytosis of β2m leads to formation of β-fibrils and subsequent lysosomal rupture. Next, we investigated the underlying mechanism by which β2m induces NLRP3 inflammasome activation. Since the NLRP3 inflammasome in macrophages is known to be activated by phagocytosis of crystals or peptides, we reasoned that phagocytosis is essential for β2m-triggered IL-1β release. Initially, we analyzed whether β2m is internalized by macrophages. Therefore, we treated macrophages with fluorescent-labeled β2m for three hours in presence or absence of the phagocytosis inhibitor cytochalasin D. Analysis by

confocal microscopy demonstrated that β2m was phagocytosed rapidly by macrophages (**Fig. 2A**, top), and that pretreatment of macrophages with cytochalasin D prevented β2m uptake (**Fig. 2A**, bottom). Similar to monosodium urate crystals (MSU), β2m-triggered release of IL-1β was also attenuated by cytochalasin D (**Fig. 2B**), which indicated that phagocytosis is required for the induction of IL-1β secretion by β2m. Cytochalasin D had no effect on the release of IL-1β after stimulation with nigericin (**Supplementary Fig. 1F**). Human β2m is known for its amyloid propensity *in vivo* (Gejyo et al., 1985) (Valleix et al., 2012) and specifically it has been shown to form amyloid-like fibrils under acidic conditions (McParland et al., 2000) (Platt and Radford, 2009). Thus, we hypothesized that after phagocytosis, β2m may aggregate in lysosomes at low pH conditions (pH4 - pH5), forms cross-β-fibrils, which lead to lysosomal rupture and the concomitant release of lysosomal factors into the cytosol, which finally activates the NLRP3 inflammasome. Firstly, we found that bafilomycin a1, an inhibitor of lysosomal acidification, prevents IL-1β release, suggesting that phagolysosome acidification is necessary for β2m-mediated inflammasome activation (**Supplementary Fig. 1G**). Secondly, we examined whether amyloids are present in macrophages after β2m internalization. Therefore, we analyzed fibril formation in β2m-treated macrophages using AmyTracker™ reagent, a cell-permeant fluorescent marker binding to fibrillar and proto-fibrillar amyloids (Klingstedt and Nilsson, 2012). Flow cytometry analysis of macrophages revealed a significant increase in amyloid structures after treatment with β2m (**Fig. 2C** and **Supplementary Fig. 1H**). Simultaneously, we detected caspase-1 activation in AmyTracker-positive macrophages indicating a connection between β-fibril formation and inflammasome activation (**Supplementary Fig. 1H**). In order to further validate whether amyloid formation of β2m is required for inflammasome induction, we tested the effect of the mutational β2m variant $\beta2m_{W60G}$ (**Fig. 2D**) on lysosomal damage and inflammasome activation in macrophages. In contrast to WT β2m, $\beta2m_{W60G}$ is reported to have greater thermodynamic stability and an overall lower aggregation propensity as compared to the WT protein

(Santambrogio et al., 2010) (Ami et al., 2012) (Camilloni et al., 2016). Specifically, *in vitro* experiments showed that at lysosomal pH between pH 4 and pH 5, $\beta2m_{W60G}$ displayed markedly low aggregation propensity and that its folded fraction was higher than the one observed for WT β2m (**Supplementary Fig. 1I**). Initially, we investigated whether β2m and $\beta2m_{W60G}$ showed differential formation of amyloid fibrils in lysosomes of macrophages. Therefore, we treated macrophages with both β2m and $\beta2m_{W60G}$ and analyzed these cells by electron microscopy. Phagocytosed β2m led to a diffused cellular distribution of fibrillar aggregates in the cytosol of macrophages (**Fig. 2E,** left), while $\beta2m_{W60G}$, was localized as globular aggregates in structurally intact lysosomes (**Fig. 2E**, right). To further explore whether lysosomal damage occurs during the phagocytosis of β2m, we simultaneously monitored lysosomal integrity and phagocytosis of labeled β2m and $\beta2m_{W60G}$ by confocal microscopy. We identified punctuated colocalization of fluorescently labeled $\beta2m_{W60G}$ with intact lysosomes by LysoTracker, a fluorescent dye, which selectively accumulates in acidic vesicular compartments, predominantly in late endosomes and lysosomes (**Fig. 2F**, right). In contrast to the mutant form, WT β2m-containing lysosomes were partially swollen and the lysomotropic dye was also detected in the cytoplasm, suggesting a destabilization of lysosomal integrity (**Fig. 2F**, left). We confirmed this findings with a LysoSensor flow cytometry-based assay in which we quantified lysosomal destabilization by the increase in LysoSensor-negative cells. Consistent with the findings obtained by confocal microscopy, β2m-treatment resulted in a loss of fluorescence, whereas treatment with $\beta2m_{W60G}$ had no effect on LysoSensor accumulation in macrophages (**Fig. 2G** and **Supplementary Fig. 1J**). Accordingly, the reduced lysosomal destabilization by $\beta2m_{W60G}$ was reflected by a significant reduction in IL-1β (**Fig. 2H**) and IL-18 release (**Supplementary Fig. 1K**) in comparison to WT β2m. We reasoned that the lysosomal destabilization results in the release of lysosomal factors, such as proteolytic enzymes or reactive oxygen species (ROS), which in turn activate the NLRP3 inflammasome (Chevriaux et al., 2020; Chu et al., 2009; Zhou et al., 2011).

Therefore, we treated macrophages with β2m or $β2m_{W60G}$ and measured intracellular cathepsins B activity with the fluorescent substrate Magic Red-(RR)2, which selectively binds to proteolytically cleaved active cathepsin B. Cathepsin B is assumed to directly induce NLRP3 inflammasome activation as well as to mediate mitochondrial (mt) dysfunction leading to mtROS-triggered NLRP3 inflammasome activation. In contrast to the control $β2m_{W60G}$, β2m treatment resulted in a diffuse cellular staining pattern, which demonstrated release of active cathepsin B into the cytosol (**Supplementary Fig. 1L**). Pretreatment of macrophages with the cathepsin B-specific inhibitor CA-074 Me resulted in a significant inhibition of IL-1β release (**Fig. 2I**), whereas the inhibitor had no effect on nigericin-mediated IL-1β release (**Supplementary Fig. 1M**). In addition, we detected increased amounts of ROS in macrophages after treatment with β2m, which could be abrogated by the ROS scavenger N-acetylcysteine (NAC) (**Fig. 2J and Supplementary Fig. 1N**). Moreover, treating macrophages with NAC inhibited the β2m-triggered release of IL-1β (**Supplementary Fig. 1N**). Collectively, these data indicate that it is not β2m internalization in lysosomes of macrophages but rather its amyloid aggregation that causes lysosomal rupture and the concomitant release of lysosomal factors, such as proteolytic enzyme cathepsin B, into the cytosol resulting in inflammasome activation.

β2m-mediates NLRP3 inflammasome activation in TAMs of MM patients.

Based on our observation that β2m can activate the NLRP3 inflammasome in macrophages, we hypothesized that MM patients with elevated β2m concentrations also display elevated inflammasome activation. To test this hypothesis, we initially correlated β2m BM plasma concentrations of MM patients with concentrations of IL-1β and IL-18. By separating IL-1β and IL-18 concentrations into low (≤ 2.7 μg/ml), intermediate (2.8 - 9.7 μg/ml), and high (≥ 9.8 μg/ml) β2m groups, we found that higher β2m concentrations resulted in increased IL-1β and IL-18 production in the BM plasma of MM patients (**Fig. 3A** and **Supplemental Figure**

2A). Next, we analyzed the local abundance of β2m in BM biopsies of MM patients and whether β2m is even more concentrated in close vicinity of MM cells and TAMs. Comparing areas with MM cell infiltration with areas without MM infiltration, we found, that β2m was enriched in the surrounding areas of MM cells (**Supplemental Figure 2B**). Furthermore, we also observed an increased β2m content in TAMs when in close contact with MM cells (**Supplemental Figure 2C**). Since macrophages are the primary sources for the release of active IL-1β and IL-18, we investigated whether these cytokines and further inflammasome associated-markers are present in TAMs of MM patients. Therefore, we isolated macrophages ($CD163^+$ and $CD15^-$) from BM aspirates harvested from the pelvic crest of healthy donors (BM macrophages of healthy controls, HD) or from MM patients (TAMs) by flow cytometry-based sorting (**Supplemental Figure 2D**). Firstly, RNA analysis of isolated TAMs of untreated MM patients showed an increased transcription of inflammasome associated-markers (AIM2, CASP1, IL-1B, IL-18, and NLRP3) in comparison to BM macrophages of healthy controls (**Fig. 3B**). Secondly, staining BM samples of untreated MM patients or benign controls for IL-1β or caspase-1 (p20) and the macrophage marker CD68, revealed an enhanced activation of caspase-1 (**Fig. 3C**, left) and high expression of IL-1β in TAMs (**Fig. 3C**, right) (**Supplemental Figure 2E**) as compared to control BM macrophages. Furthermore, the same picture emerged in comparison with TAMs of diffuse large B-cell lymphoma (DLBCL) patients (**Supplemental Fig. 3A and B**). Next, we compared the expression of inflammasome markers in TAMs of MM patients with BM macrophages of healthy donors by flow cytometry (**Fig. 3D**). We found that, in comparison to healthy control macrophages, TAMs displayed a significant increased expression of NLRP3, IL-1β, and IL-18. However, we detected by flow cytometry only a slight increase in caspase-1 activation. We further corroborated the notion that TAMs of MM patients display an active inflammasome by additional experiments. First, we identified ASC foci in TAMs of MM patients, strongly indicative of inflammasome activation. These foci were absent in BM macrophages of healthy

controls or TAMs of DLBCL patients, hinting towards an MM specific effect. Moreover, we found that only TAMs of MM patients (and not of healthy controls or DLBCL patients) secreted high amounts of IL-1β and IL-18 (**Supplemental Fig. 3C and D**). In order to analyze whether amyloid fibrils are present in TAMs of MM patients, we stained TAMs with AmyTracker™ to visualize amyloid proteins and FLICA to detect simultaneously active caspase-1. Analysis by flow cytometry demonstrated, that amyloidogenic proteins were present in TAMs of MM patients, but not in BM macrophages from healthy controls (**Fig. 3E and Supplemental Fig. 3E**). Furthermore, a high proportion of amyloid-positive TAMs displayed also an active caspase-1, suggesting a link between the presence of amyloid proteins and inflammasome activation (**Fig. 3E**; **Supplemental Fig. 3E**). To verify that TAMs contain increased amounts of amyloid fibrils, we performed dot blot analyses by using conformation-specific antibodies against cross-β fibrils or against soluble β2m (**Supplemental Fig. 3F**). We detected high amyloid concentrations in cell lysates of isolated TAMs, but not in the healthy control macrophages (**Fig. 3F**). Conversely, the amount of soluble β2m was less in TAMs, which together could indicate a shift from the soluble to the aggregated compartment. Of note, the conformation-specific antibody against amyloid fibrils recognizes generic epitopes common to many amyloid fibrils and fibrillar oligomers, but not monomers, prefibrillar oligomers or natively folded proteins. Next, we sought to determine, whether β2m in BM plasma of MM patients has the ability to activate caspase-1 and to subsequently promote IL-1β and IL-18 release. Therefore, we primed *in vitro* generated macrophages with LPS and treated them with BM plasma of untreated MM patients in the presence or absence of a neutralizing anti-β2m antibody. We detected by flow cytometry a robust increase in caspase-1 activation in macrophages after stimulation with BM plasma of MM patients (**Fig. 3G**). Moreover, treatment of macrophages with BM plasma of MM patients also led to an increase of IL-1β and IL-18 release (**Fig. 3H**). These effects were markedly inhibited in the presence of the neutralizing anti-β2m antibody, whereas isotype

control treatment had no effect (**Supplementary Fig. 3G**). In contrast, treatment with BM plasma of healthy donors induced neither an increase in caspase-1 activation nor an increase in IL-1β or IL-18 release. However, when we spiked BM plasma of healthy donors with β2m we observed IL-1β and IL-18 secretion (**Supplemental Fig. 3H, I and J**). Collectively, this data indicates that β2m in the BM plasma of MM patients is responsible for inflammasome activation in macrophages and for the release of IL-1β and IL-18.

β2m-triggers NLRP3 inflammasome activation *in vivo*.

To elucidate whether β2m is responsible for inflammasome activation in MM, we investigated the induction of the inflammasome in the 5TGM1-model. The 5TGM1-model reflects characteristic clinical features of human MM. When transplanting myeloma cells (5TGM1) into immune competent syngeneic mice, recipients develop a monoclonal protein and osteolytic bone lesions, inevitably leading to hind limb paralysis. Initially, syngeneic GFP positive myeloma cells (5TGM1) were injected in C57BL/KaLwRijHsd mice and serum concentration of β2m, IL-1β, and IL-18 were determined weekly for four weeks (**Fig. 4A**). Amounts of β2m, IL-1β, and IL-18 increased with the stage of MM (**Fig. 4A, 4B** and **Supplemental Fig. 4A**), which is in accordance with our observation in patients. In addition, we observed an increase in IL-6 and TNF (**Supplemental Fig. 4B**). Next, we analyzed mRNA expression of isolated (murine) TAMs and found, that, similar to human TAMs, BM macrophages of 5TGM1 bearing mice, expressed high amounts of NLRP3 mRNA in comparison to controls (**Fig. 4C**). Moreover, flow cytometric analysis of these TAMs demonstrated high expression of IL-1β and IL-18 during tumor progression, similar to patient TAMs (**Supplemental Fig. 4C**). Because we found that β2m forms aggregates in lysosomes leading to NLRP3 inflammasome activation, we next investigated whether amyloid fibrils might be present in BM macrophages of 5TGM1 bearing mice (**Fig. 4D**). Flow cytometry demonstrated an increase in amyloid-positive BM macrophages from 5TGM1 bearing mice,

which was not the case for BM macrophages of control mice (**Supplemental Fig. 4D**). Simultaneously, we detected an enhanced caspase-1 activation in amyloid-positive BM macrophages, confirming the connection between β2m aggregation and NLRP3 inflammasome activation in this murine MM model (**Fig. 4D; Supplemental Fig. 4E**). To decipher whether β2m is responsible for the observed inflammasome induction, we generated β2m low expressing 5TGM1 cells by transduction with shRNA against β2m (**Fig. 4E** and **Supplemental Fig. 4F and G**) and injected these cells into syngeneic mice. In line with previous data, we quantified high serum concentration of IL-1β and IL-18 in late stage of disease. In contrast, we detected only low amounts of IL-1β and IL-18 in mice challenged with β2m low expressing 5TGM1 cells (**Fig. 4F**). Compared with the control group, silencing β2m in 5TGM1 cells inhibited the formation of amyloid aggregates in TAMs and the activation of caspase-1 (**Fig. 4G**). These data indicate that β2m of myeloma cells is at least partly responsible for inflammasome activation in MM.

Inhibition of the NLRP3 inflammasome reduces MM progression

Due to the fact that MM cells are critically dependent on stromal and cytokine support, we reasoned that the NLRP3 inflammasome, activated by β2m aggregates, plays a pivotal role in MM progression. We therefore co-cultured 5TGM1 cells with BM of NLRP3-deficient mice ($Nlrp3^{-/-}$) or BM of control mice (C57BL/KaLwRijHsd) and measured MM cell growth using flow cytometry. When MM cells were cultured with BM of C57BL/KaLwRijHsd mice, an increase in cell numbers was measured after 24 hours (**Fig. 5A**). In contrast, BM cells of NLRP3-deficient mice failed to support cell growth of MM cells (**Fig. 5B**). Furthermore, activation of the AIM2 inflammasome in BM of NLRP3-deficient mice restored stromal growth support of MM cells, suggesting that inflammatory effector molecules are required for the promotion of MM cell growth (**Fig. 5C**). To confirm the requirement of an active NLRP3 inflammasome for the stromal growth support, we blocked the NLRP3 inflammasome with

the selective NLRP3 inhibitor MCC950 (Coll et al., 2015). Treatment of BM and MM cells with MCC950 resulted in a reduction of MM cell growth (**Fig. 5D**). Of note, we did not observe direct cytotoxic effects of MCC950 on MM cell growth (**Supplemental Fig. 5A**). We next sought to address the mechanism of NLRP3-dependent growth support. BM cells were incubated with MM cells in the presence of various blocking antibodies (anti-IL-1β, anti-IL-6, anti-IL-18 or anti-IL-18 receptor), and MM cell growth was determined by flow cytometry. Growth support was markedly inhibited in the presence of an anti-IL-18 or an anti-IL-18 receptor antibody, whereas anti-isotype control treatment had no effect (**Fig. 5E** and **Supplemental Fig. 5B**). Conversely, the inhibition of IL-1β or IL-6 in the co-culture did not result in a reduction of stromal growth support (**Supplemental Fig. 5B**). By analyzing the IL-1 receptor superfamily (IL1-R1, IL-18R1, and IL-1R4) on MM cells, we found that human and murine MM cells expressed high amounts of the IL-18 receptor, indicating that IL-18 could affect MM cells (**Supplemental Fig. 5C and 5D).** Treatment of 5TGM1 cells with recombinant IL-18 resulted in an increase of cell growth **(Supplemental Fig. 5E)**. In summary, these findings suggest that the observed stromal growth support depends on the inflammasome-mediated IL-18 secretion of BM cells.

Next, we investigated the effects of MCC950 on MM progression *in vivo*. Syngeneic GFP positive myeloma cells were injected in C57BL/KaLwRijHsd mice subsequently treated with MCC950. Treatment with MCC950 reduced serum concentration of IL-1β and IL-18 (**Fig. 5F**) but did not decrease the amount of TNF (**Supplementary Fig. 5F**). However, serum concentrations of IL-6 were also reduced by MCC950 treatment (**Supplementary Fig. 5F**). To determine whether MCC950 treatment also reduce MM growth *in vivo*, we measured the percentage of GFP positive myeloma cells in the BM. We found a lower percentage of myeloma cells in the BM of treated mice (**Fig. 5G** and **Supplementary Fig. 5G**). In order to measure tumor burden of MCC950-treated mice, we analyzed the serum concentrations of the monoclonal paraprotein IgG2b by ELISA in 5TGM1 tumor bearing mice receiving the

NLRP3 inhibitor MCC950 or the control group (vehicle) (**Fig. 5H**). Moreover, to measure disease severity in 5TGM1 bearing mice during MCC950 treatment, we developed a clinical scoring system ranging from 0 (asymptomatic) to 50 based on weight loss, motility, development of paralysis, and mortality. Treatment of mice with MCC950 delayed the onset and reduced the severity of MM progression (**Supplemental Fig. 5H**). Moreover, MCC950 treatment prevented development of hind limb paralysis (**Fig. 5I**). To examine osteolysis, we analyzed the femurs for bone density and volume by micro-computed tomography (μCT) (**Fig.5J**). Quantitative μCT analysis showed that injection of 5TGM1 cells induced osteolysis, (decrease in trabecular bone volume, number of trabeculae, increase in trabecular separation), whereas MCC950 treated mice display only small osteolytic lesions.

In summary, these findings strongly indicate that inflammasome activation favors MM progression, and that therapeutic inhibition of the NLRP3 inflammasome delays the onset and reduces the severity of MM.

Discussion

Inflammation is a key component of the tumor microenvironment in MM. Consequently, inflammatory TAMs promote disease progression (Kim et al., 2012), bone destruction (Roussou et al., 2009) and immune-impairment (Minnie and Hill, 2020). Our work here has identified β2m amyloid aggregation as an endogenous mediator that leads to NLRP3 inflammasome activation, resulting in exaggerated IL-1β and IL-18 secretion, which in turn promotes progression and severity of MM. Therefore, we propose, that β2m is a clinically relevant endogenous danger signal that is sensed by the NLRP3 inflammasome.

In MM patients, high concentrations of β2m correlate with poor prognosis and poor therapy response (Greipp et al., 2005) (Palumbo et al., 2015) (Bataille et al., 1984). Here, we provide one explanation for this clinical observation, by describing a β2m-triggered inflammasome activation in TAMs, which leads to increased tumor growth of MM cells and osteolytic bone

disease, a frequent complication of multiple myeloma (Terpos et al., 2013). The finding that β2m induces inflammasome activation after phagocytosis is supported by an earlier report that uptake of β2m by myeloid cells induce a pro-inflammatory immune response (Miyata et al., 1994). However, while the β2m plasma concentrations of MM patients are rarely above 10 µg/ml, we observed an increased β2m content in TAMs when in close contact with MM cells**.** Moreover, a role of the inflammasome complex in MM was previously suggested by one elegant study, using Vk*MYC mice. Injection of Vk12653 MM cells in *NLRP3*$^{-/-}$, *ASC*$^{-/-}$ or *NLRP1*$^{-/-}$ resulted in prolonged survival compared to WT mice (Nakamura et al., 2018).

Here, we have shown that β2m uptake was necessary for the activation of the NLRP3 inflammasome but its accumulation in lysosomes was not *per se* sufficient as amyloid aggregation was required. Indeed, while NLRP3 inflammasome was activated in macrophages treated with WT β2m, the single mutant $\beta2m_{W60G}$, known to be highly stable and poorly amyloidogenic (Camilloni et al., 2016) (Ami et al., 2012) (Santambrogio et al., 2010), failed to trigger the same effect. According *in vitro* experiments at pH values mimicking lysosomal environment showed that under such conditions $\beta2m_{W60G}$ tended to retain its native structure and form little aggregates while the WT protein was largely unfolded and aggregated rapidly and abundantly**.** Moreover, specific amyloid staining showed that the presence of fibrillar aggregates in macrophages treated with WT β2m was accompanied by profound lysosomal damage and NLRP3 inflammasome activation. Conversely, a clear correlation between absence of amyloids, intact lysosomes, and lacking activation of NLRP3 inflammasome was observed in macrophages treated with $\beta2m_{W60G}$**.** Taking together, these data strongly support β2m amyloid aggregation as the molecular event responsible for lysosomal rupture and ultimately for the activation of NLRP3 inflammasome.

Our results support a model in which induction of the NLRP3 inflammasome in TAMs triggered by "frustrated phagocytosis" is a critical and early step in the initiation and progression of MM. In fact, the most common cancer associated with Gaucher disease, a

primary macrophage lysosomal storage disorder characterized by chronic macrophages activation and overproduction of IL-1β, is MM (Ayto and Hughes, 2013). Along with our observations, this is consistent with inflammasome induction by lysosomal damage playing a key role in the development of MM. Moreover, increased β2m serum concentrations are also observed in a range of autoimmune, renal, and hematological diseases. For example, elevated serum β2m concentrations have been reported in rheumatoid arthritis (RA) (Sjoblom et al., 1980) or inflammatory bowel disease (IBD) (Descos et al., 1979). In both diseases tissue macrophages exhibit a hyper-activated NLRP3 inflammasome complex and increased amounts of IL-1β and IL-18 are detected in active RA (Guo et al., 2018) or IBD (Zhen and Zhang, 2019). Regarding our observation, that β2m aggregation activates the NLRP3 inflammasome in TAMs, it is tempting to speculate that β2m amyloids may be a general trigger for NLRP3 inflammasome activation in a range of otherwise unrelated inflammatory diseases. Moreover, this work suggests that human amyloidogenic proteins may not solely be looked as the causes of several incurable human diseases but also their potentially toxic behavior may play an aggravating role in diseases unrelated with amyloid aggregation.

Both IL-1β and IL-18, which are abundant in the serum of MM patients, have already been linked to the pathogenesis of MM. IL-1β promotes inflammatory osteolysis, regulates the homing of malignant plasma cells into the BM, and controls IL-6 production, which is important for myeloma cell survival and proliferation (Lust and Donovan, 1999). Importantly, treatment with a recombinant IL-1R antagonist (Anakinra) prolongs the progression-free survival of patients with indolent myeloma, suggesting that therapeutic reduction of IL-1β activity can halt progression to active MM (Lust et al., 2009). In contrast, much less is known about the pathologic functions of IL-18 in MM. High concentrations of BM plasma IL-18 were associated with poor overall survival of MM patients (Alexandrakis et al., 2004) and mice deficient for IL-18 were protected from Vk*MYC MM progression. Moreover, IL-18

can accelerate generation of myeloid-derived suppressor cells (MDSCs), which in turn inhibit T cell-mediated killing of MM cells (Nakamura et al., 2018).

We observed increased cell growth of MM cells in the presence of BM cells, which was abrogated by blocking IL-18 signaling and inhibition of the NLRP3 inflammasome. However, treatment of 5TGM1 cells with recombinant IL-18 only resulted in a minor increase in cell growth. This suggests that IL-18 alone is not sufficient to induce proliferation of MM cells. However, the observation that IL-18 directly affects MM cells is supported by previous findings of IL-18 injection in mice resulting in the production of self-reactive antibodies and expansion of plasma cells (Enoksson et al., 2011). IL-18 also facilitates bone destruction by stimulating osteoclast formation through upregulation of RANKL (receptor activator of nuclear factor κB ligand) (Dai et al., 2004). However, IL-18 frequently appears to act synergistically with other factors, and it is frequently unclear whether IL-18-associated effects are direct and/or indirect effects.

Even though we demonstrate that uptake and amyloid aggregation of β2m can trigger inflammasome activation in MM, the question of which factors aid in priming the inflammasome in this disease remains open. Although high concentrations of β2m alone were able to replace LPS as the priming agent, the amount of secreted IL-1β and IL-18 concentrations was much lower under these conditions, implicating the involvement of other factors. However, recent studies indicate that certain endogenous ligands, which were recognized by Toll-like receptors (TLRs), are expressed in the tumor microenvironment. For example, the extracellular matrix proteoglycan versican has previously been shown to activate TLR2- and TLR6-signaling in myeloma-associated macrophages (Hope et al., 2014). It remains to be determined, whether there are other damage-associated molecular patterns (DAMPs), like syndecan-1 (Yang et al., 2007) or S100 proteins (De Veirman et al., 2017), in MM, able to induce a non-infectious inflammatory response.

The 5TGM1-model revealed that activation of TAMs by β2m increased tumor growth and lytic bone lesions. These effects are strongly reduced in the presence of the specific NLRP3 inhibitor MCC950 (Coll et al., 2015). These results have important practical ramifications in light of ongoing clinical trials specifically investigating inhibition of inflammasome components in human cancers (Karki and Kanneganti, 2019). Although some clinical trials focusing on the inhibition of the downstream effector IL-1β showed promising results (Ridker et al., 2017) (Lust et al., 2009), blocking IL-1β or IL-18 individually have been shown to increase the risk of infections. Theoretically, specific inhibition of one inflammasome-type such as NLRP3 (by e.g. MCC950) could block pathological effects of NLRP3 without compromising the beneficial effects from other inflammasomes. This approach appears particularly promising as our results highlight β2m-tiggered inflammasome induction as a relevant pathophysiological process mediating inflammatory bone destruction. Importantly, morbidity, mortality as well as, the overall quality of life of MM patients is directly linked to progressive osteolytic bone disease, which is a hallmark of MM. The results from our study demonstrated that inflammasome inhibition during MM progression reduces osteolytic lesions, which is in accordance with earlier reports (Mbalaviele et al., 2017). Mechanistically, IL-1β can directly or indirectly induce osteoclast differentiation and targeting IL-1β limits osteolysis in inflammatory diseases (Dinarello et al., 2012). Moreover, mice with an activating mutation in the NLRP3 gene exhibit systemic inflammation and severe osteopenia (Qu et al., 2015). In this context, it is notable that thalidomide, a well-established drug in the front line therapy of MM, can inhibit caspase-1, which suggests that the anti-neoplastic effects of this agent may be mediated (at least partially) through inflammasome inhibition (Keller et al., 2009). However, given that an active inflammasome triggers tumor growth, immune escape, and osteolytic lesions, we expect that targeted inflammasome inhibition during standard treatment will improve outcome and wellbeing of patients with MM.

Taken together, our data allow building a model describing the molecular events supporting inflammation in MM. β2m is abundantly internalized by macrophages and lysosomal environment facilitates β2m aggregation. The accumulation of amyloid fibrils results in lysosomal damage and subsequent inflammasome induction and thereby MM progression. We may speculate that such molecular cascade could be relevant beyond MM, and that this work may extend the understanding of the β2m-mediated inflammasome activation also in other inflammatory diseases.

Limitations of study

While we have shown that β2m can activate the inflammasome, the concentrations used have been higher than in most patient-derived serum samples. Furthermore, we need to take into consideration that additional factors contribute to the observed pro-inflammatory skewing. Since β2m can accumulate in autoimmune disorders and other B-cell-derived malignancies, we need to delineate its broader pathological impact. Finally, due to the pleiotropic anti-tumor effects of IL-18, future studies must show whether its blockade is effective in MM patients.

Acknowledgements

H.B. was supported by Wilhelm-Sander Foundation and by the German Research Foundation (DFG BR 4775/2-1). S.V. was supported by the Research Foundation Medicine at the University Clinic Erlangen, Germany. Martina Maritan is kindly acknowledged for technical help. Graphical Abstract was created with the help of Designs that Cell (www.designsthatcell.ca). This work was partially supported by Fondazione ARISLA (project TDP-43-STRUCT) and by Fondazione Telethon (GGP17036) to SR. We thank the Core Unit Cell Sorting and Immunomonitoring Erlangen for supporting the work.

Authorship Contributions

D.H. performed experiments, helped writing manuscript. D.M. conceived project, designed the experiments and helped writing manuscript. M.B.H. selected and evaluated histopathological MM specimens, established the immunohistochemical staining. L.B., C.M.G.D.L, K.B., M.B., C.F., C.V. and F.M. designed and performed experiments. C.B. F.N., R.Z., S.H., S.V., J.V. B.S., S.H. and M.E. provided patient materials, mouse tissue, analyzed data and provided critical suggestions and discussions throughout the study. S.B. and J.N. designed and performed animal experiments. M.Z. contributed essential reagents/analytical tools and scientific input. A.M. provided major intellectual input for project design, helped writing the manuscript. S.R. conceived project designed the experiments and wrote the manuscript. H.B. conceived and directed the project, wrote manuscript.

Declaration of Interest

Heiko Bruns received research support from Celgene and Morphosys. All other authors declared no conflict of interest.

References

Alexandrakis, M.G., Passam, F.H., Sfiridaki, K., Moschandrea, J., Pappa, C., Liapi, D., Petreli, E., Roussou, P., and Kyriakou, D.S. (2004). Interleukin-18 in multiple myeloma patients: serum levels in relation to response to treatment and survival. Leuk Res *28*, 259-266.

Alexanian, R., Barlogie, B., and Dixon, D. (1986). High-dose glucocorticoid treatment of resistant myeloma. Ann Intern Med *105*, 8-11.

Ami, D., Ricagno, S., Bolognesi, M., Bellotti, V., Doglia, S.M., and Natalello, A. (2012). Structure, stability, and aggregation of beta-2 microglobulin mutants: insights from a Fourier transform infrared study in solution and in the crystalline state. Biophys J *102*, 1676-1684.

Ayto, R., and Hughes, D.A. (2013). Gaucher disease and myeloma. Crit Rev Oncog *18*, 247-268.

Bataille, R., Grenier, J., and Sany, J. (1984). Beta-2-microglobulin in myeloma: optimal use for staging, prognosis, and treatment--a prospective study of 160 patients. Blood *63*, 468-476.

Bjorkman, P.J., Saper, M.A., Samraoui, B., Bennett, W.S., Strominger, J.L., and Wiley, D.C. (1987). Structure of the human class I histocompatibility antigen, HLA-A2. Nature *329*, 506-512.

Camilloni, C., Sala, B.M., Sormanni, P., Porcari, R., Corazza, A., De Rosa, M., Zanini, S., Barbiroli, A., Esposito, G., Bolognesi, M*., et al.* (2016). Rational design of mutations that change the aggregation rate of a protein while maintaining its native structure and stability. Sci Rep *6*, 25559.

Chevriaux, A., Pilot, T., Derangere, V., Simonin, H., Martine, P., Chalmin, F., Ghiringhelli, F., and Rebe, C. (2020). Cathepsin B Is Required for NLRP3 Inflammasome Activation in Macrophages, Through NLRP3 Interaction. Front Cell Dev Biol *8*, 167.

Chu, J., Thomas, L.M., Watkins, S.C., Franchi, L., Nunez, G., and Salter, R.D. (2009). Cholesterol-dependent cytolysins induce rapid release of mature IL-1beta from murine macrophages in a NLRP3 inflammasome and cathepsin B-dependent manner. J Leukoc Biol *86*, 1227-1238.

Coll, R.C., Robertson, A.A., Chae, J.J., Higgins, S.C., Munoz-Planillo, R., Inserra, M.C., Vetter, I., Dungan, L.S., Monks, B.G., Stutz, A*., et al.* (2015). A small-molecule inhibitor of the NLRP3 inflammasome for the treatment of inflammatory diseases. Nat Med *21*, 248-255.

Coussens, L.M., and Werb, Z. (2002). Inflammation and cancer. Nature *420*, 860-867.

Dai, S.M., Nishioka, K., and Yudoh, K. (2004). Interleukin (IL) 18 stimulates osteoclast formation through synovial T cells in rheumatoid arthritis: comparison with IL1 beta and tumour necrosis factor alpha. Ann Rheum Dis *63*, 1379-1386.

De Veirman, K., De Beule, N., Maes, K., Menu, E., De Bruyne, E., De Raeve, H., Fostier, K., Moreaux, J., Kassambara, A., Hose, D*., et al.* (2017). Extracellular S100A9 Protein in Bone Marrow Supports Multiple Myeloma Survival by Stimulating Angiogenesis and Cytokine Secretion. Cancer Immunol Res *5*, 839-846.

Descos, L., Andre, C., Beorghia, S., Vincent, C., and Revillard, J.P. (1979). Serum levels of beta-2-microglobulin--a new marker of activity in Crohn's disease. N Engl J Med *301*, 440-441.

Dinarello, C.A., Simon, A., and van der Meer, J.W. (2012). Treating inflammation by blocking interleukin-1 in a broad spectrum of diseases. Nat Rev Drug Discov *11*, 633-652.

Durie, B.G., Vela, E.E., and Frutiger, Y. (1990). Macrophages as an important source of paracrine IL6 in myeloma bone marrow. Curr Top Microbiol Immunol *166*, 33-36.

Enoksson, S.L., Grasset, E.K., Hagglof, T., Mattsson, N., Kaiser, Y., Gabrielsson, S., McGaha, T.L., Scheynius, A., and Karlsson, M.C. (2011). The inflammatory cytokine IL-18 induces self-reactive innate antibody responses regulated by natural killer T cells. Proc Natl Acad Sci U S A *108*, E1399-1407.

Esposito, G., Ricagno, S., Corazza, A., Rennella, E., Gumral, D., Mimmi, M.C., Betto, E., Pucillo, C.E., Fogolari, F., Viglino, P*., et al.* (2008). The controlling roles of Trp60 and Trp95 in beta2-microglobulin function, folding and amyloid aggregation properties. J Mol Biol *378*, 887-897.

Gejyo, F., Yamada, T., Odani, S., Nakagawa, Y., Arakawa, M., Kunitomo, T., Kataoka, H., Suzuki, M., Hirasawa, Y., Shirahama, T., and et al. (1985). A new form of amyloid protein associated with chronic hemodialysis was identified as beta 2-microglobulin. Biochem Biophys Res Commun *129*, 701-706.

Greipp, P.R., San Miguel, J., Durie, B.G., Crowley, J.J., Barlogie, B., Blade, J., Boccadoro, M., Child, J.A., Avet-Loiseau, H., Kyle, R.A.*, et al.* (2005). International staging system for multiple myeloma. J Clin Oncol *23*, 3412-3420.

Guo, C., Fu, R., Wang, S., Huang, Y., Li, X., Zhou, M., Zhao, J., and Yang, N. (2018). NLRP3 inflammasome activation contributes to the pathogenesis of rheumatoid arthritis. Clin Exp Immunol *194*, 231-243.

Halabelian, L., Ricagno, S., Giorgetti, S., Santambrogio, C., Barbiroli, A., Pellegrino, S., Achour, A., Grandori, R., Marchese, L., Raimondi, S.*, et al.* (2014). Class I major histocompatibility complex, the trojan horse for secretion of amyloidogenic beta2-microglobulin. J Biol Chem *289*, 3318-3327.

Halle, A., Hornung, V., Petzold, G.C., Stewart, C.R., Monks, B.G., Reinheckel, T., Fitzgerald, K.A., Latz, E., Moore, K.J., and Golenbock, D.T. (2008). The NALP3 inflammasome is involved in the innate immune response to amyloid-beta. Nat Immunol *9*, 857-865.

Hamarsheh, S., and Zeiser, R. (2020). NLRP3 Inflammasome Activation in Cancer: A Double-Edged Sword. Front Immunol *11*, 1444.

He, Y., Hara, H., and Nunez, G. (2016). Mechanism and Regulation of NLRP3 Inflammasome Activation. Trends Biochem Sci *41*, 1012-1021.

Hebron, E., Hope, C., Kim, J., Jensen, J.L., Flanagan, C., Bhatia, N., Maroulakou, I., Mitsiades, C., Miyamoto, S., Callander, N.*, et al.* (2013). MAP3K8 kinase regulates myeloma growth by cell-autonomous and non-autonomous mechanisms involving myeloma-associated monocytes/macrophages. Br J Haematol *160*, 779-784.

Hideshima, T., Chauhan, D., Schlossman, R., Richardson, P., and Anderson, K.C. (2001). The role of tumor necrosis factor alpha in the pathophysiology of human multiple myeloma: therapeutic applications. Oncogene *20*, 4519-4527.

Hope, C., Ollar, S.J., Heninger, E., Hebron, E., Jensen, J.L., Kim, J., Maroulakou, I., Miyamoto, S., Leith, C., Yang, D.T.*, et al.* (2014). TPL2 kinase regulates the inflammatory milieu of the myeloma niche. Blood *123*, 3305-3315.

Hornung, V., Bauernfeind, F., Halle, A., Samstad, E.O., Kono, H., Rock, K.L., Fitzgerald, K.A., and Latz, E. (2008). Silica crystals and aluminum salts activate the NALP3 inflammasome through phagosomal destabilization. Nat Immunol *9*, 847-856.

Karki, R., and Kanneganti, T.D. (2019). Diverging inflammasome signals in tumorigenesis and potential targeting. Nat Rev Cancer *19*, 197-214.

Kawano, Y., Moschetta, M., Manier, S., Glavey, S., Gorgun, G.T., Roccaro, A.M., Anderson, K.C., and Ghobrial, I.M. (2015). Targeting the bone marrow microenvironment in multiple myeloma. Immunol Rev *263*, 160-172.

Keller, M., Sollberger, G., and Beer, H.D. (2009). Thalidomide inhibits activation of caspase-1. J Immunol *183*, 5593-5599.

Kim, J., Denu, R.A., Dollar, B.A., Escalante, L.E., Kuether, J.P., Callander, N.S., Asimakopoulos, F., and Hematti, P. (2012). Macrophages and mesenchymal stromal cells support survival and proliferation of multiple myeloma cells. Br J Haematol *158*, 336-346.

Klingstedt, T., and Nilsson, K.P. (2012). Luminescent conjugated poly- and oligo-thiophenes: optical ligands for spectral assignment of a plethora of protein aggregates. Biochem Soc Trans *40*, 704-710.

Latz, E., Xiao, T.S., and Stutz, A. (2013). Activation and regulation of the inflammasomes. Nat Rev Immunol *13*, 397-411.

Lightfield, K.L., Persson, J., Brubaker, S.W., Witte, C.E., von Moltke, J., Dunipace, E.A., Henry, T., Sun, Y.H., Cado, D., Dietrich, W.F.*, et al.* (2008). Critical function for Naip5 in inflammasome activation by a conserved carboxy-terminal domain of flagellin. Nat Immunol *9*, 1171-1178.

Lust, J.A., and Donovan, K.A. (1999). The role of interleukin-1 beta in the pathogenesis of multiple myeloma. Hematol Oncol Clin North Am *13*, 1117-1125.

Lust, J.A., Lacy, M.Q., Zeldenrust, S.R., Dispenzieri, A., Gertz, M.A., Witzig, T.E., Kumar, S., Hayman, S.R., Russell, S.J., Buadi, F.K.*, et al.* (2009). Induction of a chronic disease state in patients with smoldering or indolent multiple myeloma by targeting interleukin 1{beta}-induced interleukin 6 production and the myeloma proliferative component. Mayo Clin Proc *84*, 114-122.

Mariathasan, S., Weiss, D.S., Newton, K., McBride, J., O'Rourke, K., Roose-Girma, M., Lee, W.P., Weinrauch, Y., Monack, D.M., and Dixit, V.M. (2006). Cryopyrin activates the inflammasome in response to toxins and ATP. Nature *440*, 228-232.

Martinon, F., Petrilli, V., Mayor, A., Tardivel, A., and Tschopp, J. (2006). Gout-associated uric acid crystals activate the NALP3 inflammasome. Nature *440*, 237-241.

Masters, S.L., Dunne, A., Subramanian, S.L., Hull, R.L., Tannahill, G.M., Sharp, F.A., Becker, C., Franchi, L., Yoshihara, E., Chen, Z*., et al.* (2010). Activation of the NLRP3 inflammasome by islet amyloid polypeptide provides a mechanism for enhanced IL-1beta in type 2 diabetes. Nat Immunol *11*, 897-904.

Mbalaviele, G., Novack, D.V., Schett, G., and Teitelbaum, S.L. (2017). Inflammatory osteolysis: a conspiracy against bone. J Clin Invest *127*, 2030-2039.

McParland, V.J., Kad, N.M., Kalverda, A.P., Brown, A., Kirwin-Jones, P., Hunter, M.G., Sunde, M., and Radford, S.E. (2000). Partially unfolded states of beta(2)-microglobulin and amyloid formation in vitro. Biochemistry *39*, 8735-8746.

Minnie, S.A., and Hill, G.R. (2020). Immunotherapy of multiple myeloma. J Clin Invest *130*, 1565-1575.

Miyata, T., Inagi, R., Iida, Y., Sato, M., Yamada, N., Oda, O., Maeda, K., and Seo, H. (1994). Involvement of beta 2-microglobulin modified with advanced glycation end products in the pathogenesis of hemodialysis-associated amyloidosis. Induction of human monocyte chemotaxis and macrophage secretion of tumor necrosis factor-alpha and interleukin-1. J Clin Invest *93*, 521-528.

Nakamura, K., Kassem, S., Cleynen, A., Chretien, M.L., Guillerey, C., Putz, E.M., Bald, T., Forster, I., Vuckovic, S., Hill, G.R*., et al.* (2018). Dysregulated IL-18 Is a Key Driver of Immunosuppression and a Possible Therapeutic Target in the Multiple Myeloma Microenvironment. Cancer Cell *33*, 634-648 e635.

Palumbo, A., and Anderson, K. (2011). Multiple myeloma. N Engl J Med *364*, 1046-1060.

Palumbo, A., Avet-Loiseau, H., Oliva, S., Lokhorst, H.M., Goldschmidt, H., Rosinol, L., Richardson, P., Caltagirone, S., Lahuerta, J.J., Facon, T*., et al.* (2015). Revised International Staging System for Multiple Myeloma: A Report From International Myeloma Working Group. J Clin Oncol *33*, 2863-2869.

Platt, G.W., and Radford, S.E. (2009). Glimpses of the molecular mechanisms of beta2-microglobulin fibril formation in vitro: aggregation on a complex energy landscape. FEBS Lett *583*, 2623-2629.

Prabhala, R.H., Pelluru, D., Fulciniti, M., Prabhala, H.K., Nanjappa, P., Song, W., Pai, C., Amin, S., Tai, Y.T., Richardson, P.G*., et al.* (2010). Elevated IL-17 produced by TH17 cells promotes myeloma cell growth and inhibits immune function in multiple myeloma. Blood *115*, 5385-5392.

Qu, C., Bonar, S.L., Hickman-Brecks, C.L., Abu-Amer, S., McGeough, M.D., Pena, C.A., Broderick, L., Yang, C., Grimston, S.K., Kading, J*., et al.* (2015). NLRP3 mediates osteolysis through inflammation-dependent and -independent mechanisms. FASEB J *29*, 1269-1279.

Rathinam, V.A., Jiang, Z., Waggoner, S.N., Sharma, S., Cole, L.E., Waggoner, L., Vanaja, S.K., Monks, B.G., Ganesan, S., Latz, E*., et al.* (2010). The AIM2 inflammasome is essential for host defense against cytosolic bacteria and DNA viruses. Nat Immunol *11*, 395-402.

Richardson, P.G., Barlogie, B., Berenson, J., Singhal, S., Jagannath, S., Irwin, D., Rajkumar, S.V., Srkalovic, G., Alsina, M., Alexanian, R*., et al.* (2003). A phase 2 study of bortezomib in relapsed, refractory myeloma. N Engl J Med *348*, 2609-2617.

Ridker, P.M., MacFadyen, J.G., Thuren, T., Everett, B.M., Libby, P., Glynn, R.J., and Group, C.T. (2017). Effect of interleukin-1beta inhibition with canakinumab on incident lung cancer in patients with atherosclerosis: exploratory results from a randomised, double-blind, placebo-controlled trial. Lancet *390*, 1833-1842.

Roussou, M., Tasidou, A., Dimopoulos, M.A., Kastritis, E., Migkou, M., Christoulas, D., Gavriatopoulou, M., Zagouri, F., Matsouka, C., Anagnostou, D., and Terpos, E. (2009). Increased expression of macrophage inflammatory protein-1alpha on trephine biopsies correlates with extensive bone disease, increased angiogenesis and advanced stage in newly diagnosed patients with multiple myeloma. Leukemia *23*, 2177-2181.

Rutella, S., and Locatelli, F. (2012). Targeting multiple-myeloma-induced immune dysfunction to improve immunotherapy outcomes. Clin Dev Immunol *2012*, 196063.

Santambrogio, C., Ricagno, S., Colombo, M., Barbiroli, A., Bonomi, F., Bellotti, V., Bolognesi, M., and Grandori, R. (2010). DE-loop mutations affect beta2 microglobulin stability, oligomerization, and the low-pH unfolded form. Protein Sci *19*, 1386-1394.

Sjoblom, K.G., Saxne, T., and Wollheim, F.A. (1980). Plasma levels of beta 2-microglobulin in rheumatoid arthritis. Ann Rheum Dis *39*, 333-339.

Sutterwala, F.S., Ogura, Y., and Flavell, R.A. (2007). The inflammasome in pathogen recognition and inflammation. J Leukoc Biol *82*, 259-264.

Suyani, E., Sucak, G.T., Akyurek, N., Sahin, S., Baysal, N.A., Yagci, M., and Haznedar, R. (2013). Tumor-associated macrophages as a prognostic parameter in multiple myeloma. Ann Hematol *92*, 669-677.

Terpos, E., Morgan, G., Dimopoulos, M.A., Drake, M.T., Lentzsch, S., Raje, N., Sezer, O., Garcia-Sanz, R., Shimizu, K., Turesson, I*., et al.* (2013). International Myeloma Working Group recommendations for the treatment of multiple myeloma-related bone disease. J Clin Oncol *31*, 2347-2357.

Valleix, S., Gillmore, J.D., Bridoux, F., Mangione, P.P., Dogan, A., Nedelec, B., Boimard, M., Touchard, G., Goujon, J.M., Lacombe, C*., et al.* (2012). Hereditary systemic amyloidosis due to Asp76Asn variant beta2-microglobulin. N Engl J Med *366*, 2276-2283.

Yang, Y., MacLeod, V., Dai, Y., Khotskaya-Sample, Y., Shriver, Z., Venkataraman, G., Sasisekharan, R., Naggi, A., Torri, G., Casu, B*., et al.* (2007). The syndecan-1 heparan sulfate proteoglycan is a viable target for myeloma therapy. Blood *110*, 2041-2048.

Zhen, Y., and Zhang, H. (2019). NLRP3 Inflammasome and Inflammatory Bowel Disease. Front Immunol *10*, 276.

Zheng, Y., Cai, Z., Wang, S., Zhang, X., Qian, J., Hong, S., Li, H., Wang, M., Yang, J., and Yi, Q. (2009). Macrophages are an abundant component of myeloma microenvironment and protect myeloma cells from chemotherapy drug-induced apoptosis. Blood *114*, 3625-3628.

Zhou, R., Yazdi, A.S., Menu, P., and Tschopp, J. (2011). A role for mitochondria in NLRP3 inflammasome activation. Nature *469*, 221-225.

Figure 1. β2m-induces the release of IL-1β and IL-18 in a caspase-1 and NLRP3-dependent matter. (A) IL-1β and IL-18 release from macrophages cultured in absence (UT, untreated, n=8) or presence of 100ng/ml LPS and treated with ATP (n=5) or nigericin (NIG, n=8) (blue bars) and increasing concentrations of β2m (n=8) (red bars) as measured by ELISA. (B) Western blot analysis of cell lysates and supernatants to detect NLRP3, pro-caspase-1, pro-IL-1β, ASC, β-actin, active caspase-1, IL-18 and IL-1β in macrophages cultured in absence (UT, untreated) or presence of LPS, NIG or β2m (n=3). (C) Confocal microscopy (top row) and flow cytometry (bottom row) of active caspase-1 using FLICA® (red) in macrophages cultured in absence (UT, untreated) or presence of LPS and treated with NIG or β2m. Cell membranes and nuclei were stained using WGA (green) and DAPI (blue), respectively (n=6). Scale bar: 20 μm. Grey histograms in the flow cytometry plots represent the isotype/unstained control. (D) IL-1β release from macrophages cultured in absence (UT) or presence of LPS and treated with NIG or β2m in the presence (red bars) and absence (blue bars) of caspase-1-specific inhibitor z-YVAD-fmk as measured by ELISA (n=5). (E) Confocal microscopy to detect ASC oligomers (red) in macrophages cultured in absence (UT) or presence of LPS and overnight-treated with NIG or β2m. Cell membranes and cell nuclei were stained using WGA (green) and DAPI (blue), respectively (n=3). Scale bar: 20 μm. (F) Quantification of confocal microscopy images in Fig. 1E to detect frequency [%] of ASC-positive macrophages (n = 3). Untreated (UT), LPS-primed and NIG-treated macrophages are shown as blue bars; β2m-treated macrophages are shown as red bars. (G) IL-1β release from murine bone marrow cells of C57BL/6 (WT) (blue bars) (n=10) and NLRP3-deficient (red bars) (n=7) mice left untreated (UT) or primed with LPS and treated with ATP, NIG, poly(dA:dT) or increasing concentrations of β2m as measured by ELISA. (H) IL-1β release from macrophages cultured in absence (UT) or presence of LPS and treated with NIG or β2m in the presence (red bars) and absence (blue bars) of NLRP3-specific inhibitor MCC950 as measured by ELISA (n=5). Results are presented as mean ± SEM. *P < 0.05, **P < 0.01, ***P < 0.001, ns: not. Please also see Figure S1.

Figure 2. Phagocytosis of β2m leads to formation of amyloid fibrils and lysosomal rupture. (A) Confocal microscopy to detect phagocytosis of β2m by macrophages primed with LPS and treated with fluorescent-labeled β2m (red) in the presence (bottom row) and absence (top row) of phagocytosis inhibitor cytochalasin D. Cell membranes and cell nuclei were stained using WGA (green) and DAPI (blue), respectively (n=4). Scale bar: 20 µm.(B) IL-1β release from macrophages cultured in absence (UT) or presence of LPS and treated with MSU (n = 4) or β2m (n = 5) in the presence (red bars) and absence (blue bars) of phagocytosis inhibitor cytochalasin D as measured by ELISA. (C) Flow cytometry using AmyTracker™ to detect amyloid fibrils and FLICA® to detect active caspase-1 in LPS-primed macrophages overnight-treated with β2m (n=3). (D) Comparison of tertiary structures of WT β2m (yellow) and β2mW60G (green) (PDB codes: 2YXF, 2Z9T). W60 residue is represented as stick model. (E) Electron microscopy to detect amyloid fibrils and lysosomal rupture in macrophages primed with LPS and overnight-treated with β2m or β2mW60G (n=2). Scale bar: 1µm. (F) Confocal microscopy to detect lysosomal rupture in macrophages primed with LPS and treated with fluorescent-labeled β2m and β2mW60G (green). Lysosomes, cell membranes and cell nuclei were stained using LysoTracker® (red), WGA (light blue) and DAPI (dark blue), respectively (n=3). Scale bar: 20 µm. (G) Flow cytometry using LysoSensor™ (red lines) to detect lysosomal rupture [%] in macrophages cultured in absence (UT) or presence of LPS and overnight-treated with MSU, β2m or β2mW60G (n=4) (H) IL-1β release from macrophages cultured in absence (UT) or presence of LPS and treated with β2m (blue bars) or β2mW60G (red bar) as measured by ELISA (n = 6). (I) IL-1β release from macrophages cultured in absence (UT) or presence of LPS and treated with MSU or β2m in the presence (red bars) and absence (blue bars) of cathepsin B-specific inhibitor CA-074 Me as measured by ELISA (n = 5). (J) Flow cytometry using CellROX® Deep Red (red lines) to detect mitochondrial dysfunction [%] in macrophages cultured in absence (UT) or presence of LPS and treated with β2m in the presence or absence of anti-oxidant and free radical scavenger NAC (n = 5). Results are expressed as mean ± SEM. *P < 0.05. Please also see Figure S1.

Figure 3. β2m-mediated NLRP3 inflammasome activation in TAMs of MM patients. (A) IL-1β and IL-18 concentrations in human BM plasma of untreated MM patients divided into low (≤ 2.7 µg/ml), intermediate (2.8 - 9.7 µg/ml) and high (≥ 9.8 µg/ml) β2m plasma concentrations as measured by ELISA. The distribution of single MM patients is indicated as blue dots. (B) CD163+ and CD15- BM macrophages of MM (n=3) and healthy donors (HD, n=3) were isolated from BM cell-aspirates by FACS-sorting (CD163+ and CD15-). RNA was isolated and mRNA expression analyzed by qPCR-based arrays. The heat map compares inflammasome-related markers between BM macrophages of MM or HD. The colors are derived from an inverted scale of housekeeping-normalized qPCR ΔCt values, with high numbers indicating high expression. (C) Confocal microscopy to detect active caspase-1 (left, red) and IL-1β (right, red) in human CD68-positive cells (green) from BM of healthy donors (HD) and untreated MM patients (MM). Cell nuclei were stained using DAPI (blue). Scale bar: 20 µm. (D) Flow cytometry to detect protein expression of NLRP3, active caspase-1 (FLICA®), IL-1β and IL-18 as MFI in human TAMs from BM of HDs (blue lines and bars) and untreated MM patients (red lines and bars). The gray histogram indicates the isotype control. The top row shows representative histograms of a total of n = 8 samples as summarized in the bottom row. (E) Flow cytometry using AmyTracker™ to detect amyloid fibrils and FLICA® to detect active caspase-1 in human TAMs (CD163-positive and CD15-negative) from BM of HDs and untreated MM patients. The density plots show one representative example of a total of 8 experiments. (F) Dot blot analysis of cell lysates to detect β2m and amyloid fibrils in isolated TAMs of HDs (HD 1-3) and untreated MM patients (MM 1-3). (G) Flow cytometry using FLICA® to detect frequency of active caspase-1-positive macrophages primed with LPS and overnight-co-cultured with human BM plasma of untreated MM patients in the presence (red bar) and absence (blue bar) of a β2m-neutralizing antibody (anti-β2m) (n = 6). (H) IL-1β and IL-18 release from macrophages primed with LPS and overnight-co-cultured with human BM plasma of untreated MM in the presence (red bars) or absence (blue bars) of a β2m-neutralizing antibody (anti-β2m) (n = 6). Results are expressed as mean ± SEM. *P < 0.05, **P < 0.01, ***P < 0.001, ns: not significant. Please also see Figure S2 and S3.

Figure 4. β2m-triggered NLRP3 inflammasome activation in vivo. (A) Concentrations of β2m, IL-1β and IL-18 in serum of 5TGM1 bearing mice at different time points during MM progression (first week = t0, second week = t1, third week = t2, fourth week = t3) as measured by ELISA (n = 4). (B) Flow cytometry to detect frequency of 5TGM1 GFP-positive cells in myeloma bearing mice at different time points during progression (n = 4). (C) Quantitative real-time PCR to detect gene expression of inflammatory associated genes in BM macrophages from C57BL/KaLwRijHsd mice (blue bars) (n=3) and 5TGM1 bearing mice (red bars) (n = 3). (D) Flow cytometry using AmyTracker™ to detect amyloid fibrils and FLICA® to detect active caspase-1 in BM macrophages from C57BL/KaLwRijHsd mice and 5TGM1 bearing mice. Density plots show one representative experiment of a total of 3 independent analysis. (E) Flow cytometric analysis of 5TGM1 cells expressing low amounts of β2m after shRNA-treatment (n=3). (F) Concentrations of IL-1β and IL-18 in serum of C57BL/KaLwRijHsd mice challenged with 5TGM1 cells transduced with control shRNA (blue bars) (n=8) or β2m shRNA (red bars) (n = 8). (G) Flow cytometry using AmyTracker™ to detect amyloid fibrils and FLICA® to detect active caspase-1 in BM macrophages from C57BL/KaLwRijHsd mice challenged with 5TGM1 cells transduced with control shRNA or β2m shRNA. Density plots show representative data of a total of 8 independent experiments. Results are expressed as mean ± SEM. *P < 0.05, ***P < 0.001, ns: not significant. Please also see Figure S4.

Figure 5. Inhibition of the NLRP3 inflammasome reduces MM progression. (A-E) Absolute cell count measured by flow cytometry of murine 5TGM1 cells co-cultured with murine BM cells from (A) C57BL/6 mice (red bar, n=8), (B) C57BL/6 mice (WT) (blue bar) or NLRP3-deficient mice (red bar) (n=4). (C) Cell count of 5TGM1 cells co-cultured with NLRP3-deficient mice in the presence (red bars) or absence (blue bars) of poly(dA:dT) (n=4). (D) Cell count of 5TGM1 cells co-cultured with BM of C57BL/6 mice in the presence (red bars) and absence (blue bars) of the NLRP3-specific inhibitor MCC950 (n=12) or (E) IL-18 and IL-18 receptor neutralizing antibodies (aIL-18, aIL-18R) (n=8). (F) Concentrations of IL-1β and IL-18 in serum (n=8) and (G) frequency of GFP-positive 5TGM1 cells in the bone marrow of C57BL/KaLwRijHsd mice treated with DMSO (blue bars) (n=10) or MCC950 (red bars) (n=10). (H) Multiple myeloma (MM) disease burden measured as serum IgG2b concentrations in 5TGM1 bearing mice receiving no treatment (n=5, blue circles) or MCC950 (n=5, red circles). IgG2b concentrations were determined by ELISA. Error bars show SEM. (I) Clinical evaluation of hind limb paralysis of vehicle (DMSO, blue bar)) or MCC950-treated (red bar) mice (n=10). (J) Bone densities in mice treated with DMSO (n = 5) or MCC950 (n = 5) as representatively shown for 5 independent experiments per group on the left and quantitatively summarized on the right depicting bone volume/total volume (%), trabecular number (mm) and trabecular separation (μm). Results are expressed as mean ± SEM. *P < 0.05, **P < 0.01, ***P < 0.001. Please also see Figure S5.

Cell culture reagents. Macrophages and murine BM cells were cultured in RPMI 1640 media supplemented with L-glutamine (2 mM), 2-mercaptoethanol (50 nM), PenStrep (160 µIU/ml penicillin, 160 ng/ml streptomycin) (GIBCO®, Thermo Fisher Scientific™, Waltham, USA), sodium pyruvate (1 mM), MEM-vitamin (0.4 %), MEM-NEAA (1 %) (PAN™ Biotech, Aidenbach, GER) and FCS (10 %) (c.c. pro, Oberdorla, GER).

Human sample studies. In accordance with the declaration of Helsinki and upon approval by the institutional ethics committee, each patient gave informed written consent prior to surgery, blood donation or bone marrow biopsy (MM and healthy donors) (Aachen: EK206/09; Erlangen: Ref. #3555, 36_12 B, 219_14B, 200_12B). For patients' characteristics and numbers please refer to Supplemental Tables 2. Upon single-cell isolation (see below), all cells were cryopreserved in culture medium containing 10% DMSO and stored in liquid nitrogen.

Preparation of macrophages. Human PBMCs were isolated from freshly drawn peripheral blood of healthy donors (University Hospital of Erlangen, Department of Transfusion Medicine and Haemostaseology, GER) by density gradient centrifugation using human Pancoll (1.077 g/ml) (PAN™ Biotech, Aidenbach, GER) and a subsequent buffy coat purification. To generate macrophages, monocytes were isolated by adherence to polystyrene in CELLSTAR® cell culture flasks (Greiner Bio-One, Kremsmünster, AUT) and cultured in the presence of Leucomax® GM-CSF (500 U/µl) (Novartis Pharma, Nürnberg, GER). After 6-7 d of culture, macrophages were detached with EDTA (1 mM) (Sigma-Aldrich®, München, GER).

Isolation of TAMs and BM macrophages from human samples and mice

BM cells from healthy donors, DLBCL patients or from MM patients were prepared from the pelvic crest. Bone marrow-derived mononuclear cells (BM-MNCs) were isolated from BM by density-gradient centrifugation using histopaque-1077 (Sigma) according to the manufacturer's instructions. BM-MNCs were stained with antibodies specific for CD163 and CD15 and TAMs or macrophages were separated by flow cytometry ($CD163^+$ and $CD15^-$). Purity was greater than 95%. Phenotype was evaluated by expression of surface markers CD163, CD15, CD16, CD32, CD36, CD64, CD86, CD172, CD204 and HLA-DR by flow cytometry.To purify BM macrophages of mice, BM cells were isolated by flushing femurs and tibias with complete RPMI1640. Aggregates were dislodged by gentle pipetting, and debris was removed by passaging the suspension through a 70-µm nylon web. Cells were washed twice with medium, adjusted to give a suspension of 10^6 cells/mL. BM cells were stained with antibodies against (GR1, CD115, F4/80) and BM macrophages were separated by flow cytometry ($GR1^-$, $CD115^+$, $F4/80^+$) Purity was greater than 90%.

Mice. NLRP3-deficient mice (*Nlrp3*$^{-/-}$) were provided by Prof. Dr. Robert Zeiser and Shaima'a Hamarsheh (Department of Medicine 1 - Medical Center, University of Freiburg, Freiburg, GER). C57BL/6 mice were purchased from The Jackson Laboratory (Bar Harbor, USA). 5TGM1 cells were from Dr. Jens Nolting and Savita Bisht-Feldmann (Department of Oncology/Hematology and Rheumatology, University Hospital Bonn, Bonn, GER). C57BL/KaLwRijHsd (Harlan) mice were challenged with 5TGM1 cells. Mouse strains were bred and housed in pathogen-free conditions. All experiments were in accordance with the guidelines set forth by the University Hospital of Erlangen and approved by the Institutional Animal Care and Use Committee.

Enzymatic proteolysis of β2m. β2m was overnight-incubated (37 °C, 5% CO_2) in 100 mM TRIS/HCl (pH 8.5) supplemented with trypsin-EDTA (Thermo Fisher Scientific™, Waltham,

USA). The reaction was quenched by the addition of FCS and the solution was sterile filtered (0.2 μm).

Protein expression and purification. Recombinant β2m and $\beta2m_{W60G}$ were expressed and purified as previously reported (Esposito et al., 2008).

Aggregation assays. Aggregation assays at different pH (2.5, 3, 3.5, 4, 4.5, 5, 7.5) were performed in reaction mix containing 50 mM sodium citrate (acidic conditions) or 50 mM sodium phosphate, 15 mM NaCl, β2m variant (40 μM) and ThT (10 μM). All reactions were performed in triplicate using black, clear-bottom, 96-well microplates. Upon seeding with preformed β2m fibrils, plates were incubated in a FLUOstar OPTIMA reader (BMG Labtech, Germany) at 37 °C, over a period of 100 h with intermittent cycles of shaking (1 min, 300 rpm, double-orbital) and rest (30 min). The ThT fluorescence intensity of the aggregates, expressed as arbitrary units (AU), was taken every 30 min using 450 ± 10 nm (excitation) and 480 ± 10 nm (emission) wavelength, with a bottom read and a gain of 1000.

LysoSensor™ Green DND-189. Intralysosomal pH was detected using the LysoSensor™ Green DND-189 kit from Thermo Fisher Scientific™ (Waltham, USA) according to the manufacturer's instructions. macrophages were seeded at 1×10^6/ml in polystyrene Falcon® round bottom tubes (Corning® LifeSciences, Corning, USA), LPS-primed (1 μg/ml, 3 h) and overnight-incubated with 250 μg/ml MSU crystals, 60 μg/ml β2m or 60 μg/ml $\beta2m_{W60G}$. Cells were washed with PBS and incubated with the LysoSensor™ Green DND-189 reagent (4 μM, 2 h) at 37 °C and 5 % CO_2. As assessed by flow cytometry, an increase in intralysosomal pH or rather lysosomal rupture was defined as decrease in fluorescence.

FLICA® 660 Caspase-1 assay. Caspase-1 activity was detected using the FLICA® 660 Caspase-1 assay kit from ImmunoChemistry Technologies (Bloomington, USA) according to

the manufacturer's instructions. macrophages were seeded at 1× 10^6/ml in polystyrene Falcon® round bottom tubes (Corning® LifeSciences, Corning, USA) for flow cytometry and on a 8 well Permanox™ Chamber Slide™ system (Thermo Fisher Scientific™, Waltham, USA) for immunohistochemistry analysis. Cells were LPS-primed (1 µg/ml, 3 h) and overnight-incubated with 10 µM nigericin, 10 µg/ml $\beta2m_{digest}$ or 10 µg/ml β2m in the presence of an anti-β2m-neutralizing antibody (clone: 2M2) (LifeSpan BioSciences, Seattle, USA) (10 µg/ml, 1 h) or β2m (10 or 60 µg/ml). For pancaspase inhibition, macrophages were pre-incubated with z-VAD-fmk (20 µM, 1 h). For β2m-blocking, macrophages were primed overnight with 100 ng/ml LPS and overnight-cultured with BM plasma from MM patients (8 %) in the presence of an anti-β2m-neutralizing antibody (clone: 2M2) (LifeSpan BioSciences, Seattle, USA) or an IgG1 antibody (clone: 12G8G11; 10 µg/ml, 1 h) as an isotype control. Cells were washed with PBS and incubated with the FLICA® 660-YVAD-fmk reagent (1:150, 30 min) at 37 °C and 5 % CO_2. As assessed by flow cytometry or confocal microscopy, caspase-1 activation was defined as increase in fluorescence.

AmyTracker™ 480. Amyloid fibrils in macrophages were detected using the AmyTracker™ 480 from EBBA Biotech (Solna, SWE) according to the manufacturer's instructions. Macrophages were seeded at 1× 10^6/ml in polystyrene Falcon® round bottom tubes (Corning® LifeSciences, Corning, USA), LPS-primed (1 µg/ml, 3 h) and overnight-incubated with 60 µg/ml β2m. Cells were washed with PBS and incubated with the AmyTracker™ 480 reagent (1:1000, 1 h) at 37 °C and 5 % CO_2. As assessed by flow cytometry, an increase in amyloids was defined as increase in fluorescence.

Probing the RT Profiler Human Inflammasome PCR Arrays. Total RNA was extracted from cell lysates (RNeasy mini kit, Qiagen) including on-column DNAse digestion (RNase-free DNase set, Qiagen). cDNA was prepared (RT² First Strand Kit, Qiagen) using a

Mastercycler Nexus (Eppendorf, Hamburg, Germany) and subjected to qPCR-based analyses of 84 inflammasome-related genes (RT² Profiler™ PCR Array, Qiagen) according to the manufacturer's instructions. Raw Ct values were corrected by subtracting the corresponding sample average of five housekeeping genes (ACTB, B2M, GAPDH, HPRT1, and RPLP0). For visualization in heat maps, ΔCt values were converted to a scale where higher values represent higher expression by subtracting them from the assumed limit of detection (33 cycles). Heat maps were drawn in R 3.6.3 using the package pheatmap.

Co-culture experiments. Murine GFP-positive 5TGM1 cells as well as BM cells from C57BL/6 or NLRP3-deficient mice were isolated. Subsequently, 1×10^4 GFP-positive 5TGM1 cells were co-cultured with 2.5×10^5 BM cells in a 24-well cell culture plate (96 h, 37 °C, 5% CO_2). Further analysis was implemented adding both specific neutralization antibodies and inhibitors after 72 h.

β2m shRNA silencing in 5TGM1 cells. For transfection, Phoenix ECO cells were incubated (37 °C, 5% CO_2) in the presence of a reaction mixture containing the β2m-specific shRNA (TR500182A, Origene, Rockville, USA) and TurboFectin (TF81001, Origene, Rockville, USA), whose virus supernatants were isolated after 24 h and 48 h. For transduction, 5TGM1 cells were overnight-incubated (37 °C, 5% CO_2) with the 24 h-virus supernatant supplemented with RetroNectin® (Takara BIO, Kusatsu, JAP). Subsequently, 5TGM1 cells were overnight-incubated (37 °C, 5% CO_2) with the 48 h-virus supernatant supplemented with RetroNectin®, washed with PBS and cultured vertically in CELLSTAR® cell culture flasks (Greiner Bio-One, Kremsmünster, AUT). After 5 d of culture, medium was renewed and puromycin (2 µg/ml) (InvivoGen, San Diego, USA) was added to eliminate non-transduced 5TGM1 cells. Finally, cells were analyzed by flow cytometry to determine

5TGM1 cells low expressing β2m, cryopreserved and applied to generate 5T33MM mice low expressing β2m.

Fluorescence experiments. β2m variants (8.5 μM) denaturation at different pH values was followed by intrinsic Trp fluorescence under the same conditions used for aggregation assays. All measurements were performed in triplicate on a Cary Eclipse spectrofluorometer (Agilent) using a QS High Precision Cell (HellmaAnalytics) with emission slit 5nm. Excitation wavelength was set to 295 nm and Trp fluorescence was monitored at 350 nm.

CellROX® Deep Red assay. mtROS in macrophages were detected using the CellROX® Deep Red assay kit from Thermo Fisher Scientific™ (Waltham, USA) according to the manufacturer's instructions. macrophages were seeded at 1×10^6/ml in polystyrene Falcon® round bottom tubes (Corning® LifeSciences, Corning, USA). For mtROS inhibition, medium of LPS-primed (100 ng/ml, 3 h) macrophages was removed, cells were washed with PBS and incubated in medium containing 5 mM NAC and 60 μg/ml β2m for 48 h. Cells were washed with PBS and incubated with the CellROX® Deep Red reagent (5 μM, 30 min) at 37 °C and 5 % CO_2. As assessed by flow cytometry, an increase in mtROS was defined as increase in fluorescence.

Magic Red® Cathepsin B assay. Cathepsin B activity in macrophages was detected using the Magic Red® Cathepsin B assay kit from ImmunoChemistry Technologies (Bloomington, USA) according to the manufacturer's instructions. macrophages were seeded at 1×10^6/ml on a 8 well Permanox™ Chamber Slide™ system (Thermo Fisher Scientific™, Waltham, USA), LPS-primed (1 μg/ml, 3 h) and incubated overnight with 60 μg/ml β2m. Cells were washed with PBS, incubated with the Magic Red® MR-$(RR)_2$ substrate (1:260, 45 min) at 37 °C and 5 % CO_2 and fixed with 4 % (vol/vol) paraformaldehyde. Cell membrane and nuclei staining

was performed using FITC-conjugated WGA (2.5 µg/ml) (Vector Laboratories, Burlingame, USA) and DAPI (Thermo Fisher Scientific™, Waltham, USA). As assessed by confocal microscopy, cathepsin B activation was defined as increase in fluorescence.

Protein labeling. β2m and $\beta2m_{W60G}$ were labeled using the AF™ 647 microscale protein labeling kit from Thermo Fisher Scientific™ (Waltham, USA) according to the manufacturer's instructions. For analysis of β2m phagocytosis and lysosomal rupture, macrophages were seeded at 1×10^6/ml on a 8 well Permanox™ Chamber Slide™ system (Thermo Fisher Scientific™, Waltham, USA), LPS-primed (1 µg/ml, 3 h) and overnight-incubated with AF™ 647-labeled β2m or $\beta2m_{W60G}$ (10µg/ml or 60 µg/ml). For inhibition of phagocytosis, macrophages were pre-incubated with cytochalasin D (5 µM, 1 h). Cells were washed with PBS and fixed with 4 % (vol/vol) paraformaldehyde. Cell membrane and nuclear staining was performed using FITC-conjugated WGA (2.5 µg/ml) (Vector Laboratories, Burlingame, USA) and DAPI. As assessed by confocal microscopy, β2m phagocytosis and fibril formation was defined as increase in fluorescence intensity.

Immunofluorescence double-stainings of FFPE samples. Formalin-fixed, paraffin-embedded (FFPE) bone marrow specimens were retrieved from the archive of the Institute of Pathology, FAU Erlangen-Nuremberg, including 5 bone biopsies with plasma cell myeloma and 5 biopsies from patients with iron deficiency anemia as controls. Double stainings were performed on FFPE material with antibodies specific for IL1-ß (1:100, ab95047, polyclonal rabbit, abcam, Cambridge, UK) or IL-18 (1:100, ab95047, polyclonal rabbit, abcam, Cambridge, UK) and CD68 (1:100, PG-M1, monoclonal mouse, Dako Cytomation, Hamburg, Germany). For antigen retrieval slides were cooked in a steam cooker (Biocarta Europe, Hamburg, Germany) for 2.5 minutes in a commercially available target retrieval solution pH6 (TRS6, Dako Cytomation). Primary antibodies were incubated over night at room

temperature. For the detection of CD68 an Alexa488-labeled goat anti mouse IgG3 secondary fluorescent antibody was used (1:500, Dianova, Hamburg Germany).

Confocal microscopy. Imaging was performed using the LSM 700 confocal microscope (Zeiss, Oberkochen, GER) at a magnification of x630. Slides were analyzed by z-stacking to generate up to 10 optical layers (0.5 µm).

ELISA. Cell culture supernatants, serum concentrations and bone marrow plasma were examined for human and murine cytokines IL-1β and IL-18 with ELISA kits from Biomatik (Cambridge, CAN), R&D Systems® (Minneapolis, USA) and Thermo Fisher Scientific™ (Waltham, USA) according to the manufacturer's instructions.

Inflammasome stimulation for secretion assays. Macrophages and bone marrow cells from NLRP3-deficient (*Nlrp3*-/-) and C57BL/ 6 mice were seeded at 1× 10^6/ml in polystyrene Falcon® 24 well plates (Corning® LifeSciences, Corning, USA), LPS-primed (1 µg/ml, 3 h) and incubated with nigericin (10 µM, 30 min), ATP (5 mM, 30 min), $\beta2m_{W60G}$ (10 µg/ml, 6 h), $\beta2m_{digest}$ (10 µg/ml, 6 h) and increasing concentrations of β2m (3, 6, 10, 30, 60 µg/ml, 6 h). For inhibition assays, medium of LPS-primed (100 ng/ml, 1 µg/ml, 3 h) macrophages and murine bone marrow cells was removed, cells were washed with PBS and incubated in medium containing appropriate inhibitors (20 µM z-YVAD-fmk, 10 µM MCC950, 3 µM bafilomycin A1, 5 µM cytochalasin D, 10 µM CA-074 Me), nigericin (10 µM, 30 min), MSU crystals (250 µg/ml, 6 h) or β2m (60 µg/ml, 6 h). For β2m-blocking, macrophages were seeded at 1× 10^6/ml in polystyrene Falcon® round bottom tubes (Corning® LifeSciences, Corning, USA), overnight-primed with 100 ng/ml LPS and overnight-cultured with bone marrow plasma from MM patients (8 %) in the presence of an anti-β2m-neutralizing antibody

(clone: 2M2) (LifeSpan BioSciences, Seattle, USA) or an anti-IgG1 antibody (clone: 12G8G11) (BioLegend®, Minneapolis, USA) (10 µg/ml, 1 h).

Flow cytometry. A FACSCanto™ II cytometer (BD Biosciences, Franklin Lakes, USA) was used for all flow cytometric assays, data were acquired by a FACSDIVA™ software (BD Biosciences, Franklin Lakes, USA) and analyzed using a FlowJo_v10 software (Tree Star, Ashland, USA).

LEGENDplex™. Serum were examined for murine IL-1β, IL-6 and TNF-α with LEGENDplex™ Mouse capture bead assay kit from BioLegend (San Diego, USA) according to the manufacturer's instructions using flow cytometry.

123count eBeads™ counting beads assay. 123count eBeads™ counting beads were used for cytometric cell quantification. Therefore, cells were resuspended in PBS, 123count eBeads ™ counting beads were added and the absolute number of cells/µl was determined using flow cytometry.

Dot blot analysis. BM cells from MM patients and HDs were examined for β2m and β-fibrils. Therefore, cell lysates were prepared by direct lysis of 2× 106 cells in ddH2O and incubation (30 min, 0°C). Cell debris was removed by centrifugation (21,400 xg, 15 min, 4 °C) and the concentration of total protein in cell extracts was determined using the Qubit® protein assay kit and the Qubit® 3.0 fluorometer (Thermo Fisher Scientific™). Cell lysates were transferred onto nitrocellulose membranes (0.2 µm) (GE Healthcare Life Sciences, Chalfont St Giles, UK) using the T790.1 dot blotter (Carl Roth, Karlsruhe, GER) (5 min, 20 °C). Subsequently, proteins were fixed on the membrane using the CL-1000 UVP crosslinker (Analytik Jena, Jena, GER) (100 µJ/cm2, 1 min, 20 °C). Membrans were blocked in 5 %

(wt/vol) dried milk in TBS-T (100 mM Tris/HCl, 150 mM NaCl, 0.1 % (vol/vol) Tween®-20) for 1 h at room temperature. Membranes were incubated with primary antibodies diluted in 5 % (wt/vol) dried milk in TBS-T (2 h, 4 °C). Subsequently, membranes were incubated with the appropriate HRP-conjugated secondary antibody diluted in 5 % (wt/vol) dried milk in TBS-T for 1 h at room temperature. Proteins were detected by chemiluminescence using the SuperSignal® ELISA femto maximum sensitivity substrate (Thermo Fisher Scientific™, Waltham, USA) according to the manufacturer's instructions and the Amersham™ Imager 600 (GE Healthcare Life Sciences, Chalfont St Giles, UK). Primary antibodies used were anti-β2m (clone: EP2978Y) (Abcam®, Cambridge, UK) and anti-amyloid fibrils LOC (Merck, Darmstadt, GER) (1:2,000). Secondary HRP-conjugated antibody used was anti-rabbit IgG (7074) (1:2,500) (Cell Signaling Technology®, Cambridge, UK).

Western blot analysis. Cell lysates and supernatants were examined for human proteins IL-1β, IL-18, NLRP3, ASC, caspase-1, β-actin and β2m. Macrophages were seeded at 2×10^6/ml in polystyrene Falcon® 24 well plates (Corning® LifeSciences, Corning, USA), LPS-primed (1 µg/ml, 3 h) and overnight-incubated with 10 µM nigericin or 60 µg/ml β2m. Cell lysates were prepared by direct lysis in 2 % (w/v) SDS lysis buffer (5 mM EDTA, 50 mM Tris/HCl, 150 mM NaCl, 2.2 % (wt/vol) SDS) supplemented with cOmplete™ EDTA-free (Roche Diagnostics, Mannheim, GER) as protease inhibitor. Cell debris was removed by centrifugation (21,382 xg, 15 min, 4 °C) and the concentration of total protein in cell extracts was determined using the Qubit® protein assay kit and the Qubit® 3.0 fluorometer (Thermo Fisher Scientific™). Cell culture supernatants were used purely. Protein samples were resuspended in 4× Laemmli sample buffer (278 mM Tris/HCl, 355 mM 2-mercaptoethanol, 0.02 % (wt/vol) bromophenol blue, 4.4 % (wt/vol) lithium dodecyl sulfate, 44.4 % (vol/vol) glycerol, pH (HCl) 6.8) (Bio-Rad Laboratories, München, GER) and boiled for 10 min at 95 °C. The protein content of cell lysates, supernatants and the Precision Plus Protein™

WesternC™ standard (Bio-Rad Laboratories, München, GER) was separated by SDS-PAGE (10 %, 15 %, 90 µg) and transferred onto nitrocellulose membranes (0.2 µm) (GE Healthcare Life Sciences, Chalfont St Giles, UK) using the semi-dry TransBlot® Turbo™ transfer system (Bio-Rad Laboratories, München, GER). Membranes were blocked in 5 % (wt/vol) dried milk in TBS-T (100 mM Tris/HCl, 150 mM NaCl, 0.1 % (vol/vol) Tween®-20) for 1 h at room temperature. Membranes were overnight-incubated with primary antibodies diluted in 5 % (wt/vol) dried milk in TBS-T at 4 °C. Subsequently, membranes were incubated with the appropriate HRP-conjugated secondary antibody diluted in 5 % (wt/vol) dried milk in TBS-T for 1 h at room temperature. Proteins were detected by chemiluminescence using the SuperSignal® ELISA femto maximum sensitivity substrate (Thermo Fisher Scientific™, Waltham, USA) according to the manufacturer's instructions and the Amersham™ Imager 600 (GE Healthcare Life Sciences, Chalfont St Giles, UK). Membranes were stripped using the Restore™ western blot stripping buffer (Thermo Fisher Scientific™, Waltham, USA) before being re-examined. Primary antibodies used were β-actin (4967) (1:2,500), caspase-1 (clone: D7F10), IL-1β (clone: 3A6), NLRP3 (clone: D2P5E) (Cell Signaling Technology®, Cambridge, UK), ASC (clone: B-3) (Santa Cruz Biotechnology®, Dallas, USA), IL-18 (ab191152) and β2m (ab6608) (1:1,000) (Abcam®, Cambridge, UK). Secondary HRP-conjugated antibodies used were anti-mouse IgG (7076) and anti-rabbit IgG (7074) (1:2,500) (Cell Signaling Technology®, Cambridge, UK).

Immunocytochemistry. Cells were fixed using 4 % (vol/vol) paraformaldehyde for 15 min at room temperature. Cell membranes were stained using FITC- or AF™ 555-conjugated WGA (2.5 µg/ml) (Vector Laboratories, Burlingame, USA) (Thermo Fisher Scientific™, Waltham, USA). Nuclear staining was performed using DAPI (Thermo Fisher Scientific™, Waltham, USA).

Electron microscopy. Cells were resuspended in PBS and fixed with 4% (vol/vol) paraformaldehyde with exclusion of light (15 min, 20 °C). Subsequently, cells were washed and resuspended in PBS, transferred to transmission electron microscopy (TEM) grids and dried (24 h, 20 °C). Then, TEM grids were washed with PBS and incubated in PBS supplemented with 2% (vol/vol) glutaraldehyde (5 min, 20 ° C). After further washing steps with ddH_2O (double distilled water), TEM grids were incubated (5 min, 20 ° C) in a filtered (0.2 µm) 3% (wt/vol) uranyl acetate solution and dried (24 h, 20 °C). Finally, cells were analyzed using the LEO 912 AB electron microscope (Zeiss, Oberkochen, GER) and the Image SP software (Zeiss, Oberkochen, GER).

ASC expression assay. macrophages were seeded at 1× 10^6/ml on a 8 well Permanox™ Chamber Slide™ system (Thermo Fisher Scientific™, Waltham, USA), LPS-primed (1 µg/ml, 3 h) and overnight-incubated with 10 µM nigericin or 60 µg/ml β2m. Cells were washed with PBS, fixed with 4 % (vol/vol) paraformaldehyde and overnight-incubated at 4 °C in a humidity chamber (LabArt, Waldbüttelbrunn, GER) with the appropriate primary ASC antibody (clone: B-3) (1:200) (Santa Cruz Biotechnology®, Dallas, USA) and the secondary anti-mouse IgG F(ab')2AF™ 555-conjugated antibody (4409) (1:400) (Cell Signaling Technology®, Cambridge, UK) diluted in PBS containing 2 % (vol/vol) FCS and 0.5 % (vol/vol) Triton® X-100. Cell membrane and nuclei staining was performed using FITC-conjugated WGA (2.5 µg/ml) (Vector Laboratories, Burlingame, USA) and DAPI (Thermo Fisher Scientific™, Waltham, USA). As assessed by confocal microscopy, ASC expression was defined as increase in fluorescence.

LysoTracker® Red DND-99. Lysosomes in macrophages were detected using the LysoTracker® Red-DND-99 kit from Thermo Fisher Scientific™ (Waltham, USA) according to the manufacturer's instructions. Macrophages were seeded at 1× 10^6/ml on a 8 well

Permanox™ Chamber Slide™ system (Thermo Fisher Scientific™, Waltham, USA), LPS-primed (1 µg/ml, 3 h) and overnight-incubated with fluorescent-labeled (AF® 647) β2m and $\beta2m_{W60G}$ (10µg/ml). Cells were washed with PBS, incubated with the LysoTracker® Red-DND-99 reagent (50 nM, 1.5 h) at 37 °C and 5 % CO_2 and fixed with 4 % (vol/vol) paraformaldehyde. Cell membrane and nuclear staining was performed using FITC-conjugated WGA (2.5 µg/ml) (Vector Laboratories, Burlingame, USA) and DAPI. As assessed by confocal microscopy, lysosomal detection was defined as increase in fluorescence.

5TGM1 bearing mice treated with MCC950. In vivo studies were performed using 8-10 weeks old female C57BL/KaLwRijHsd (Harlan, Horst, The Netherlands) mice. All animal experiments described here were approved by the Government of the State of North Rhine - Westphalia and conducted in accordance with the Federation of European Laboratory Animal Science Associations (FELASA) guidelines. Myeloma was propagated in these mice by intravenous inoculation of 5 x 105 5TGM1-GFP tagged cells in 300 µl of phosphate buffered saline (PBS). After 2 weeks, mice were randomised into two groups: MCC950 treated mice and vehicle only control mice. MCC950 treated mice received drug dissolved in PBS at a dose of 10 mg/kg/BW intraperitoneally every other day. Vehicle only control mice received only PBS solution. During the course of experiment, mice were monitored regularly for any adverse events and body weights were taken twice weekly. At 3-4 week of treatment, when the vehicle controls showed signs of morbidity, the experiment was terminated . To determine the tumour load, bone marrow flushed from mice femurs were analysed immediately for GFP expression using flow cytometry. Serum was also collected and used for further analysis. Tumor burden was measured by serum IgG2bκ ELISA (ThermoFisher),

5TGM1 bearing mice treated with MCC950. In vivo studies were performed using 8-10 weeks old female C57BL/KaLwRijHsd (Harlan, Horst, The Netherlands) mice. All animal experiments described here were approved by the Government of the State of North Rhine - Westphalia and conducted in accordance with the Federation of European Laboratory Animal Science Associations (FELASA) guidelines. Myeloma was propagated in these mice by intravenous inoculation of 5 x 105 5TGM1-GFP tagged cells in 300 µl of phosphate buffered saline (PBS). After 2 weeks, mice were randomised into two groups: MCC950 treated mice and vehicle only control mice. MCC950 treated mice received drug dissolved in PBS at a dose of 10 mg/kg/BW intraperitoneally every other day. Vehicle only control mice received only PBS solution. During the course of experiment, mice were monitored regularly for any adverse events and body weights were taken twice weekly (for the scoring system please refer to Supplemental Tables 2). At 3-4 week of treatment, when the vehicle controls showed signs of morbidity, the experiment was terminated . To determine the tumor load, bone marrow flushed from mice femurs were analyzed immediately for GFP expression using flow cytometry. Serum was also collected and used for further analysis. Tumor burden was measured by serum IgG2bκ ELISA (ThermoFisher),

Quantification and statistical analysis. Results are presented as average values ± SEM from multiple independent experiments each performed at least in triplicate. The number of biological replicates are indicated as n in the Figure legends. Outliers were determined using the ROUT test. Differences in means were evaluated with parametric (paired/unpaired t-test, one-way ANOVA) or nonparametric (unpaired Mann-Whitney, paired Wilcoxon, unpaired Kruskal-Wallis) tests based on the number of comparisons (two or more than two) and distribution levels (as determined by Shapiro-Wilk and Kolmogorov-Smirnov). All statistical analyses were performed using GraphPad Prism Version 5 (GraphPad Prism Software Inc., La

Jolla, USA) or Excel 2016 (Microsoft Corp., Redmond, USA) at a significance level of * $p \leq 0.05$, ** $p \leq 0.01$, *** $p \leq 0.001$.

Supplemental Table 1: Patients' characteristics, Related to Figure 3, Figure S2 and Figure S3.

Table S1

Supplemental Table 1: Patients' characteristics				
Case No.	Donor [HD/MM]	Sex [m/f]	Age [years]	Therapy
1	MM	f	66	Newly diagnosed MM
2	MM	f	70	Newly diagnosed MM
3	MM	m	57	Newly diagnosed MM
4	MM	m	47	Newly diagnosed MM
5	MM	f	56	Newly diagnosed MM
6	MM	m	61	Newly diagnosed MM
7	MM	f	83	Newly diagnosed MM
8	MM	m	81	Newly diagnosed MM
9	MM	f	70	Newly diagnosed MM
10	MM	f	72	Newly diagnosed MM
11	MM	f	63	Newly diagnosed MM
12	MM	m	61	Newly diagnosed MM
13	MM	f	77	Newly diagnosed MM
14	MM	m	60	Newly diagnosed MM
15	MM	m	73	Newly diagnosed MM
16	MM	m	54	Newly diagnosed MM
17	MM	m	58	Newly diagnosed MM
18	MM	m	65	Newly diagnosed MM
19	MM	m	78	Newly diagnosed MM
20	MM	f	78	Newly diagnosed MM
21	MM	m	63	Newly diagnosed MM
22	MM	m	76	Newly diagnosed MM
23	MM	m	68	Newly diagnosed MM
24	MM	f	77	Newly diagnosed MM
25	MM	m	56	Newly diagnosed MM
26	MM	m	80	Newly diagnosed MM
27	MM	m	84	Newly diagnosed MM
28	MM	m	45	Newly diagnosed MM
29	MM	m	56	Newly diagnosed MM
30	MM	m	48	Newly diagnosed MM
31	MM	m	63	Newly diagnosed MM
32	MM	m	50	Newly diagnosed MM
33	MM	m	69	Newly diagnosed MM
34	MM	m	76	Newly diagnosed MM
35	MM	m	83	Newly diagnosed MM
36	MM	m	66	Newly diagnosed MM
37	MM	m	74	Newly diagnosed MM
38	MM	m	69	Newly diagnosed MM
39	MM	f	71	Newly diagnosed MM
40	MM	m	76	Newly diagnosed MM
41	MM	m	70	Newly diagnosed MM
42	MM	m	78	Newly diagnosed MM
43	MM	m	71	Newly diagnosed MM
44	MM	m	65	Newly diagnosed MM
45	MM	f	81	Newly diagnosed MM
46	MM	m	81	Newly diagnosed MM
47	MM	f	69	Newly diagnosed MM

48	MM	m	77	Newly diagnosed MM
49	MM	m	76	Newly diagnosed MM
50	MM	m	59	Newly diagnosed MM
51	MM	m	77	Newly diagnosed MM
52	MM	f	68	Newly diagnosed MM
53	MM	m	61	Newly diagnosed MM
1	HD	m	63	-
2	HD	f	21	-
3	HD	f	22	-
4	HD	f	21	-
5	HD	m	41	-
6	HD	m	26	-
7	HD	m	29	-
8	HD	m	63	-
1	DLBCL	f	47	Newly diagnosed DLBCL
2	DLBCL	f	57	Newly diagnosed DLBCL
3	DLBCL	f	61	Newly diagnosed DLBCL
1	HD plasma	m	63	-
2	HD plasma	m	69	-
3	HD plasma	m	63	-
4	HD plasma	f	68	-
5	HD plasma	m	72	-
Patients' characteristics (Immunohistochemistry)				
FFPE01	control	m	60	-
FFPE02	control	f	83	-
FFPE03	control	m	75	-
FFPE04	control	m	79	-
FFPE05	control	f	44	-
FFPE06	MM	f	65	newly diagnosed MM
FFPE07	MM	f	76	newly diagnosed MM
FFPE08	MM	f	67	newly diagnosed MM
FFPE09	MM	m	62	newly diagnosed MM
FFPE10	MM	m	60	newly diagnosed MM

Figure_1

Click here to access/download;Figure;Figure_1.tif

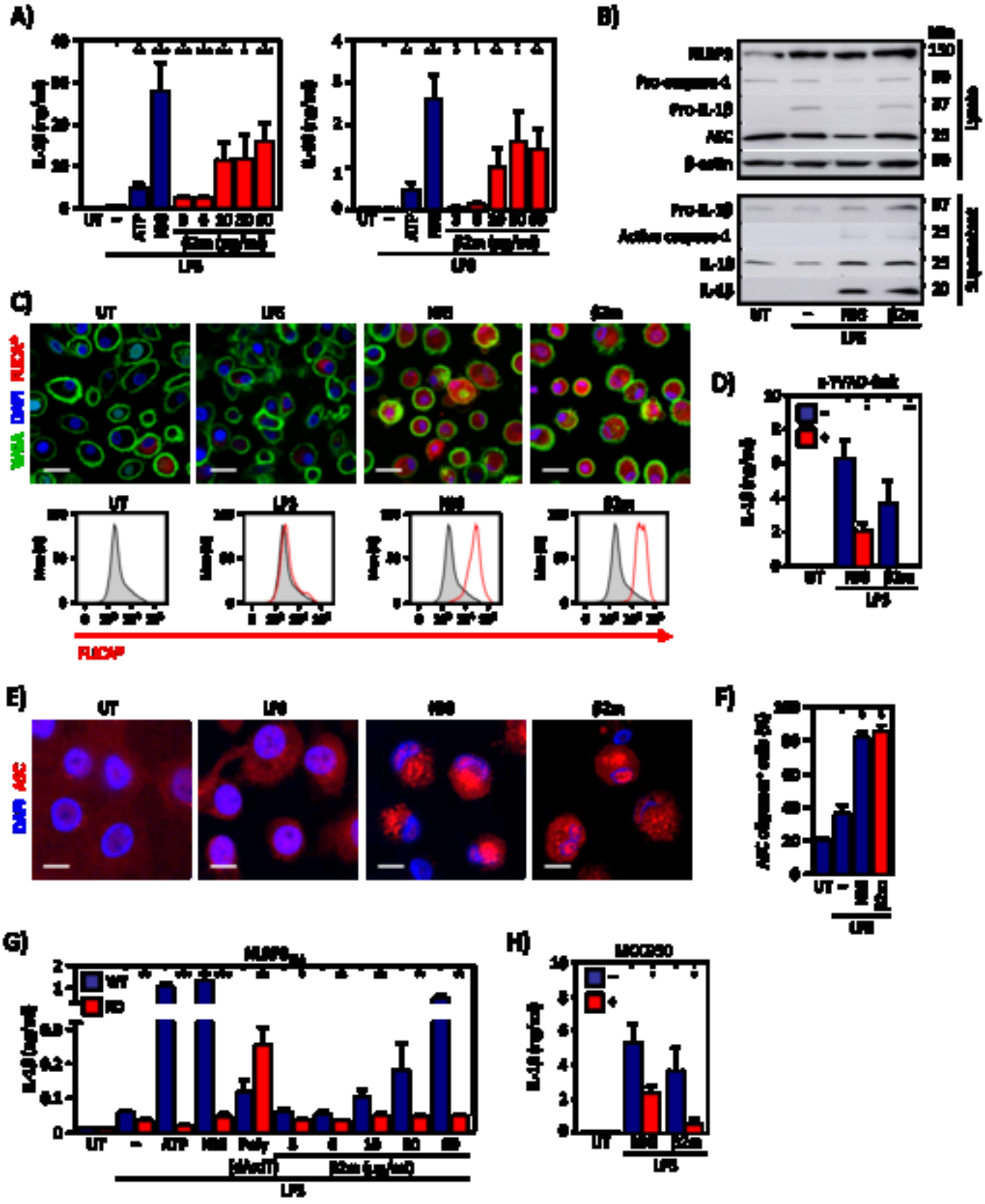

Figure_2

Click here to access/download;Figure;Figure_2.tif

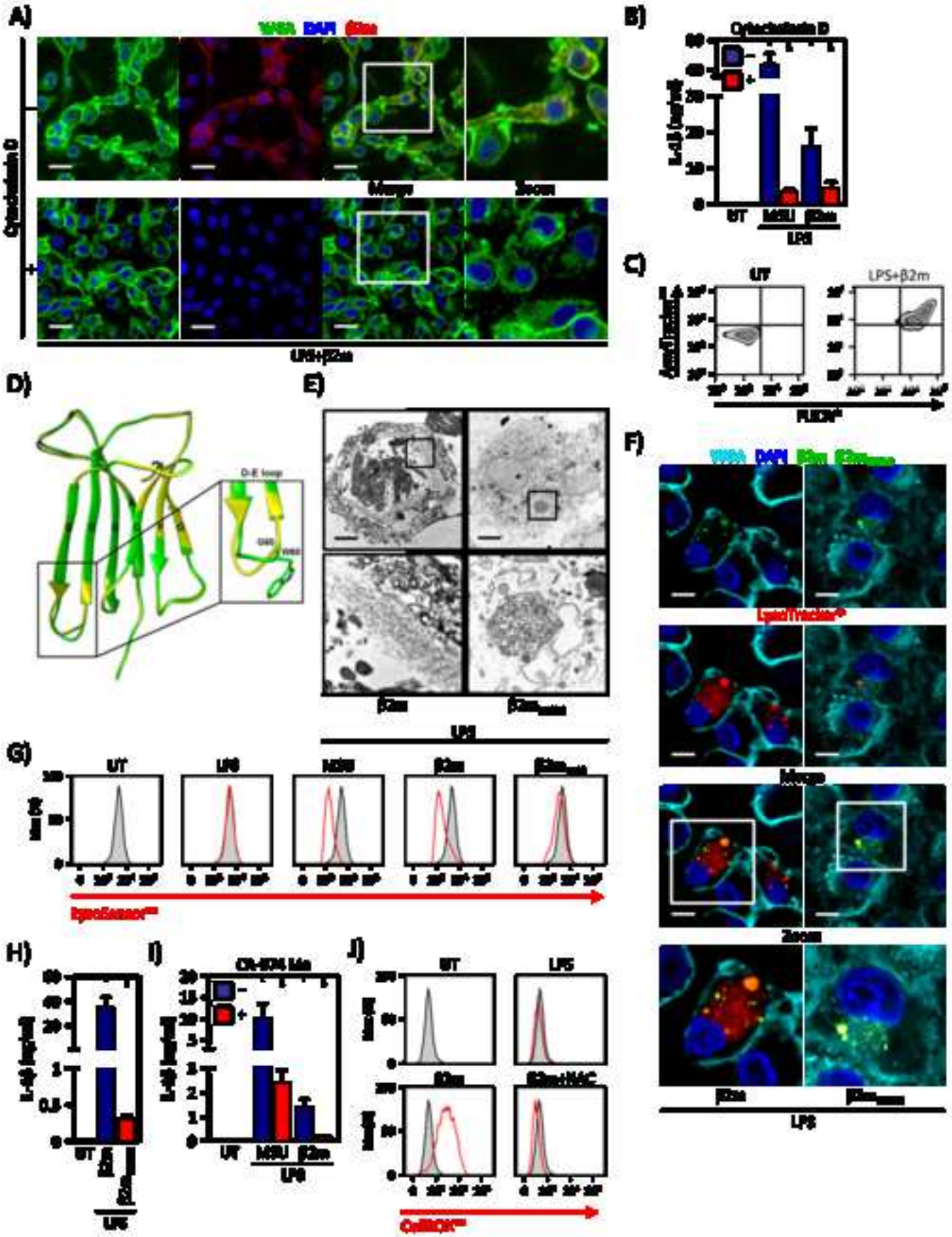

Figure_3

Click here to access/download;Figure;Figure_3.tif

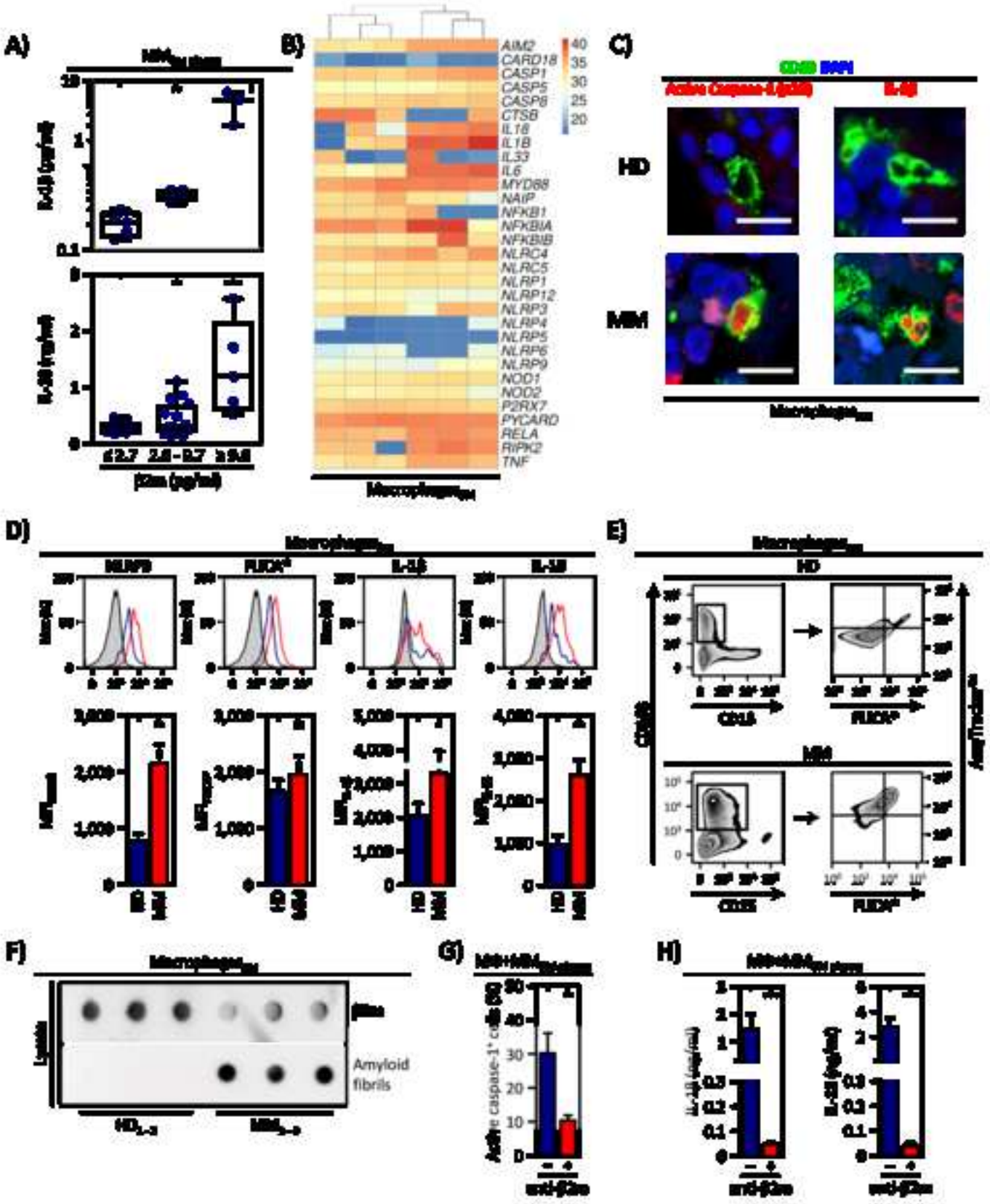

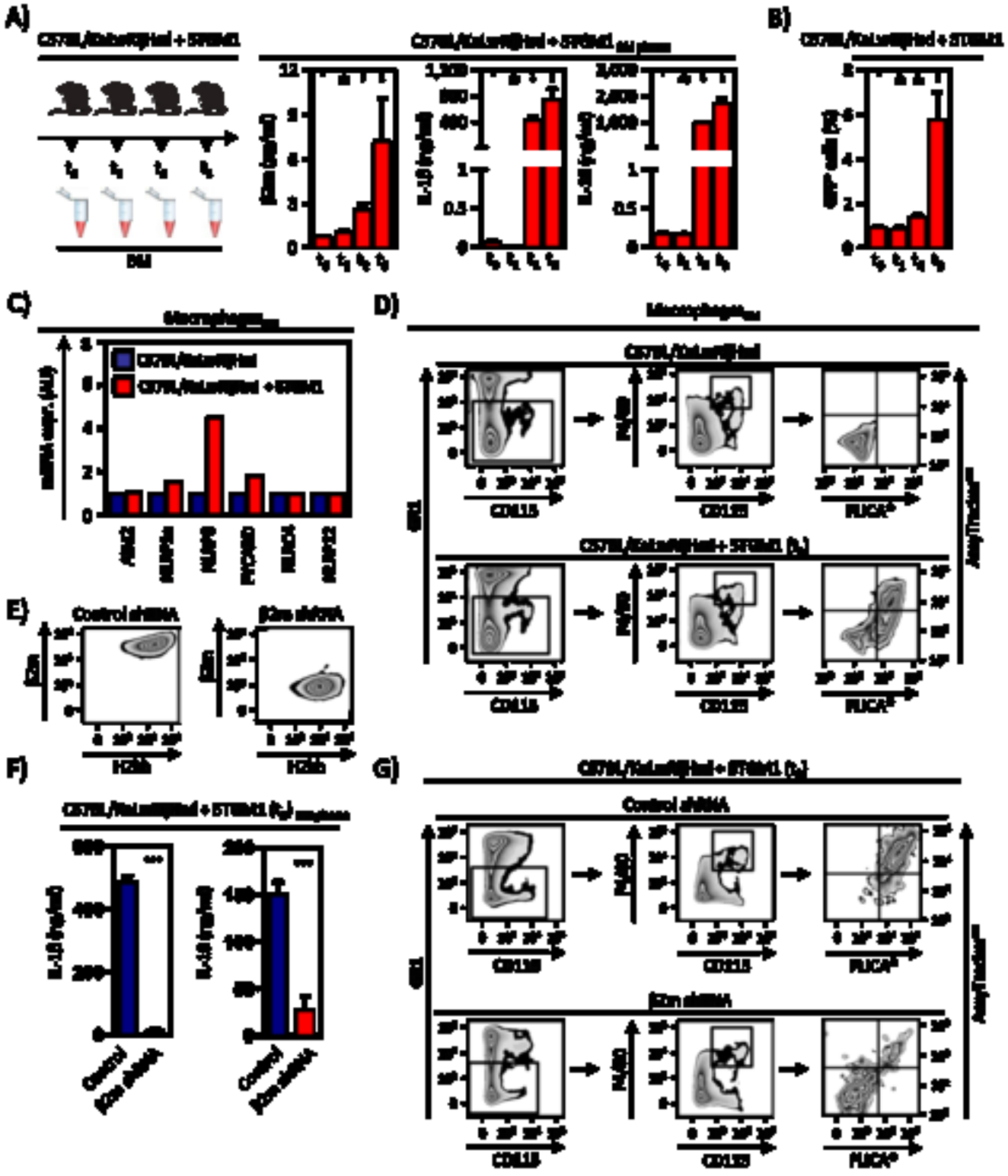

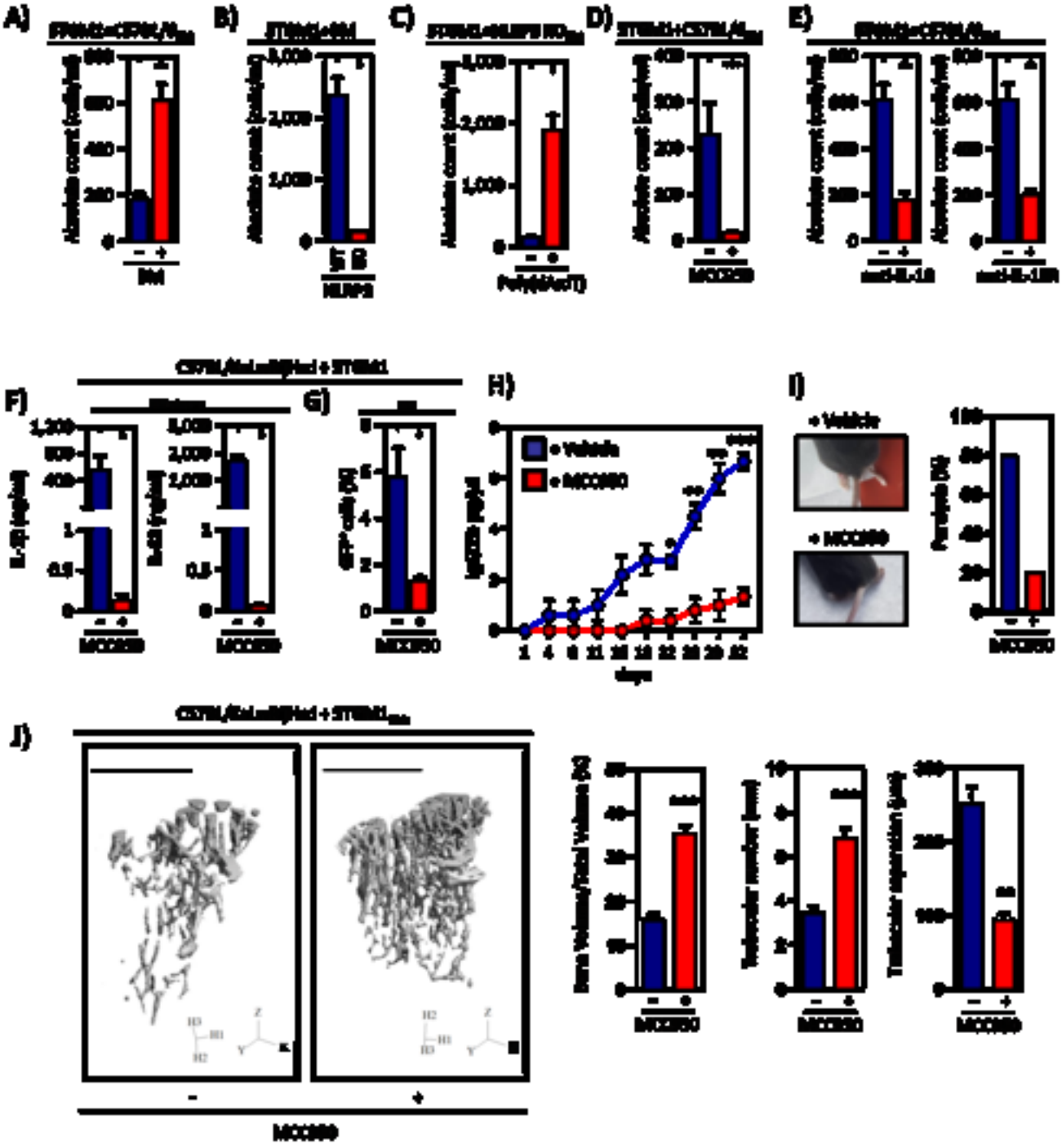

Supplemental

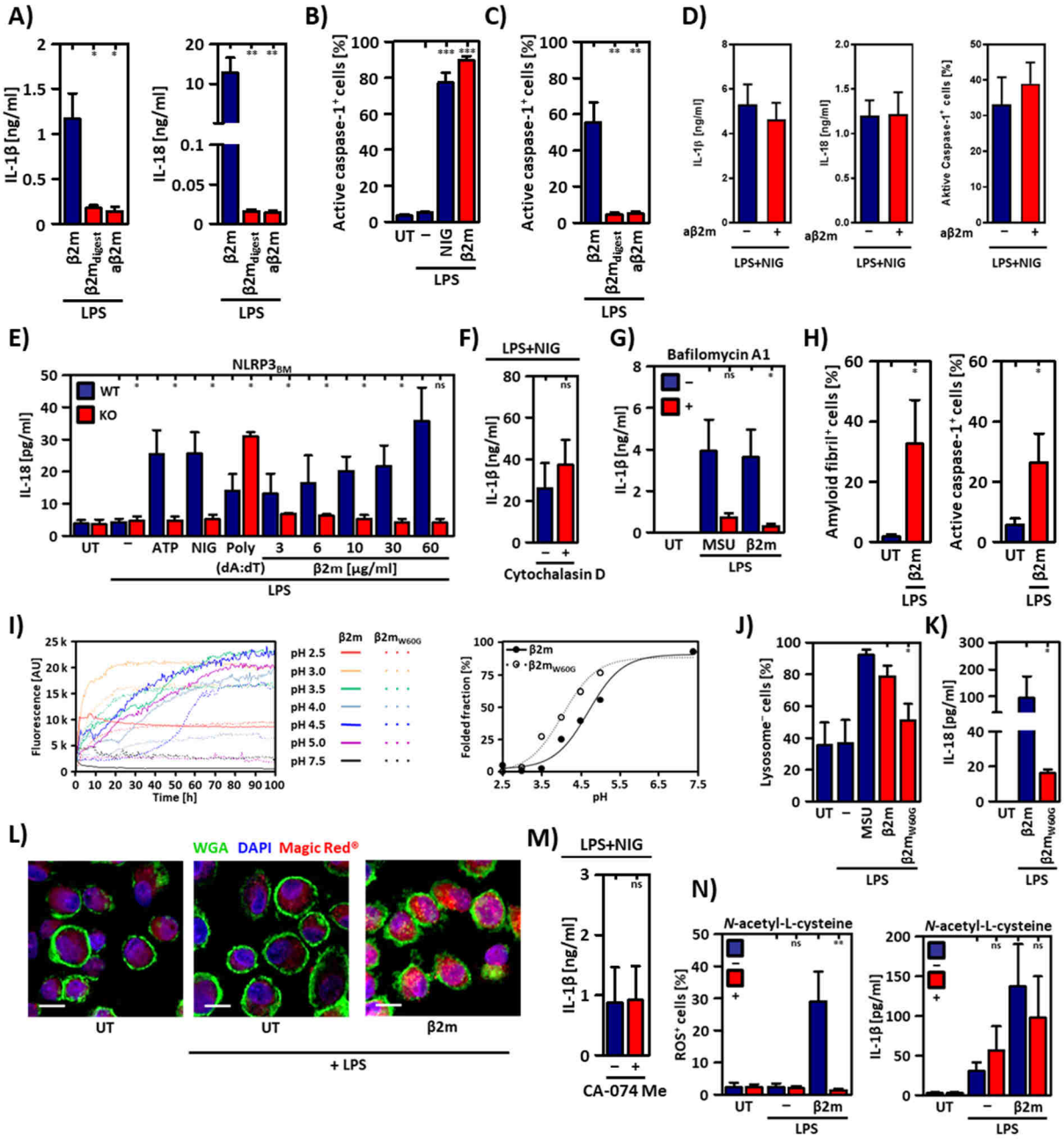

Supplementary Figure 1
β2m-induced IL-1β and IL-18 release from macrophages in a NLRP3-dependent matter, related to Figure 1 and Figure 2. (**A**) IL-1β and IL-18 release [ng/ml] from macrophages primed with LPS (100 ng/ml, 3 h) and treated for 6h with 10 µg/ml of either β2m (blue bar), $β2m_{digest}$ or β2m in the presence of a β2m-neutralizing antibody (aβ2m, 10 µg/ml) (red bars) as measured by ELISA (n = 5). (**B**) Flow cytometry using FLICA® 660 to detect percentage [%] of active caspase-1-positive macrophages left untreated (UT) or primed with LPS (100ng/ml, 3 h) and overnight-treated with nigericin (NIG, 10 µM, n = 8) (blue bars) and β2m (60 µg/ml, n = 9) (red bar) as well as (**C**) macrophages primed with LPS (100 ng/ml, 3 h) and treated for 6h with 10 µg/ml β2m (blue bar), $β2m_{digest}$ and β2m in the presence of a β2m neutralizing antibody (aβ2m, 10µg/ml) (red bars) (n = 7). (**D**) Macrophages were primed with LPS (100 ng/ml, 3 h) and treated with nigericin (NIG, 10µM, 2h) in the presence (aβ2m, 10µg/ml, red bars) or

absence (blue bars) of a β2m neutralizing antibody. IL-1β and IL-18 release was measured by ELISA, and active caspase-1 was detected with FLICA® by FACS (n=5). (**E**) IL-18 release [pg/ml] from murine bone marrow cells of C57BL/6 (WT) (blue bars) and NLRP3-deficient (KO) (red bars) mice left untreated (UT) or primed with LPS (1 µg/ml, 3 h) and treated with ATP (5 mM, 30 min), NIG (10 µM, 30 min), poly(dA:dT) (1 µg/ml, 24 h) and increasing concentrations of β2m (3, 6, 10, 30, 60 µg/ml, 6 h) as measured by ELISA (n =6). (**F**) IL-1β release [ng/ml] from macrophages primed with LPS (100 ng/ml, 3 h) and treated with Nigericin (NIG) (10 µM, 30 min) in the presence (red bar) and absence (blue bar) of phagocytosis inhibitor cytochalasin D (5 µM) as measured by ELISA (n = 5). (**G**) IL-1β release [ng/ml] from macrophages left untreated (UT) or primed with LPS (100 ng/ml, 3 h) and treated with MSU (250 µg/ml, 6 h) and β2m (60 µg/ml, 6 h) in the presence (red bars) and absence (blue bars) of V-ATPase inhibitor bafilomycin A1 (3 µM) as measured by ELISA (n = 5). (**H**) Flow cytometry using AmyTracker™ 480 and FLICA® 660 to detect percentage [%] of (C) amyloid fibril-positive and (D) active caspase-1-positive macrophages LPS-primed (blue bars) and overnight-treated with β2m (60 µg/ml) (red bars) (n = 5). (**I**) Left graph: Fluorescence spectroscopy in the ThT binding assay to detect kinetics [AU] of amyloid fibril formation of β2m (solid lines) and $\beta2m_{W60G}$ (dash lines). Right graph: Unfolding [%] of β2m (solid line, full circles) and β2mW60G (dash line, empty circles) is representative as a function of pH. Data representative of three independent experiments are shown. (**J**) Flow cytometry using LysoSensor™ Green to detect percentage [%] of lysosome negative macrophages left untreated (UT) or primed with LPS (100ng/ml, 3 h) and overnight-treated with MSU (250 µg/ml, n = 5) (blue bars), β2m (10 µg/ml, n = 6) and $\beta2m_{W60G}$ (10 µg/ml, n = 5) (red bars). (**K**) IL-18 release [pg/ml] from macrophages left untreated (UT) or primed with LPS (1 µg/ml, 3 h) and treated with β2m (blue bars) and $\beta2m_{W60G}$ (red bar) (10 µg/ml, 6 h) as measured by ELISA (n = 5). (**L**) Confocal microscopy using MAGIC RED® (red) to detect cathepsin B in macrophages left untreated (UT) or primed with LPS (1 µg/ml, 3 h) and overnight-treated with β2m (60 µg/ml). Cell membranes and cell nuclei were stained using WGA (FITC, green) and DAPI (blue), respectively. Scale bar: 20 µm. Data representative of three independent experiments are shown. (**M**) IL-1β release [ng/ml] from macrophages primed with LPS (100 ng/ml, 3 h) and treated with Nigericin (NIG, 10 µM, 30 min) in the presence (red bar) and absence (blue bar) of cathepsin B-specific inhibitor CA-074 Me (10 µM) as measured by ELISA (n = 5). (**N**) Left graph: Flow cytometry using CellROX® Deep Red to detect percentage [%] of ROS-positive macrophages left untreated (UT) or primed with LPS (100 ng/ml, 3 h, n = 4) and treated with β2m (60 µg/ml, 48 h, n = 5) in the presence (red bars) and absence (blue bars) of anti-oxidant and free radical scavenger N-acetyl-l-cysteine (NAC) (5 mM). Right graph: IL-1β release [pg/ml] from macrophages left untreated (UT) or primed with LPS (100 ng/ml, 3 h, n = 3) and treated with β2m (60 µg/ml, 6 h, n = 5) in the presence (red bars) and absence (blue bars) of NAC (5 mM) as measured by ELISA. Results are expressed as mean ± SEM. *P < 0.05, **P < 0.01, ***P < 0.001. ns: not significant.

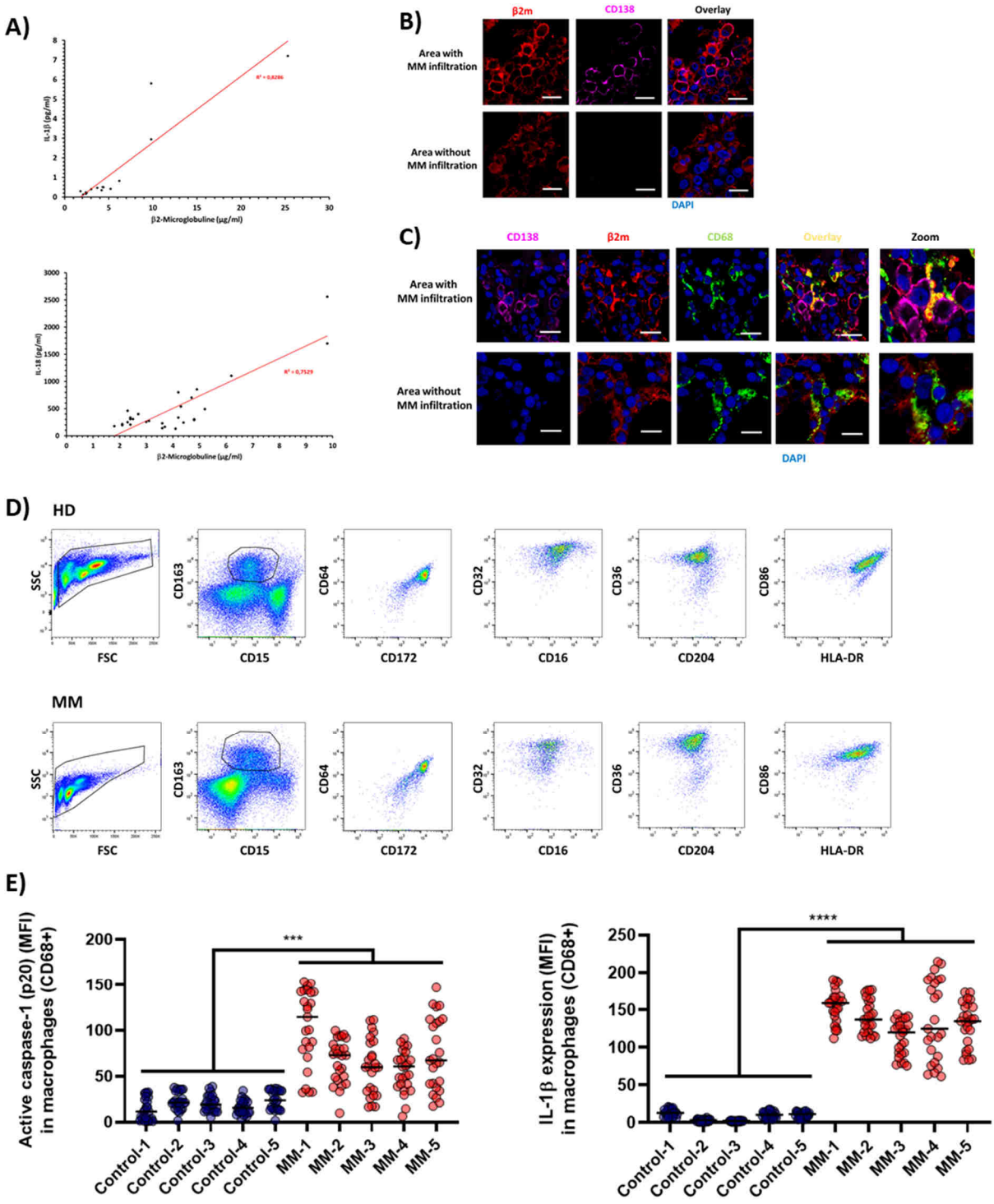

Supplementary Figure 2

Phenotype of TAMs of MM patients, related to Figure 3. **(A)** IL-1β [pg/ml] (n=15) and IL-18 [pg/ml] (n=31) levels in human BM plasma of untreated MM patients were correlated with β2m plasma concentrations as measured by ELISA. (**B**) BM biopsies of patients with multiple myeloma (MM) (n=10) were stained for ß2m (red) and CD138 (purple, MM cells). Areas with or without MM cell infiltration were analyzed for ß2m expression. (**C**) BM biopsies of MM patients were stained for CD138 (purple, MM cells), ß2m (red), and CD68 (green, macrophages). Areas with or without MM cell infiltration were analyzed for ß2m expression. Nuclei were counter-stained with DAPI. Scale bar: 10 µm. (**D**) CD163+CD15- macrophages

were isolated from BM-derived cell aspirated by FACS-based sorting. Surface markers typically found on BM-resident macrophages were assessed by FACS as representatively shown for (upper panel) a healthy donor (HD) and (lower panel) a patient with MM. (**E**) Active caspase-1 (p20) and IL1β expression in BM macrophages of benign controls (blue circles) or of MM patients (red circles). Expression of active caspase-1 or IL1β in macrophages was calculated from microscopically counted CD68+ macrophages (minimum 25 per donor, n = 5). Plots show the mean fluorescence intensity (MFI) for active caspase-1 (p20) (left) or IL1β (right) in CD68+ macrophages (each circle represents the individual active caspase-1/ IL1β MFI of a single macrophage). Lines indicate the mean values of the results. Results are expressed as mean ± SEM. *P < 0.05, **P < 0.01, ***P < 0.001. ns: not significant.

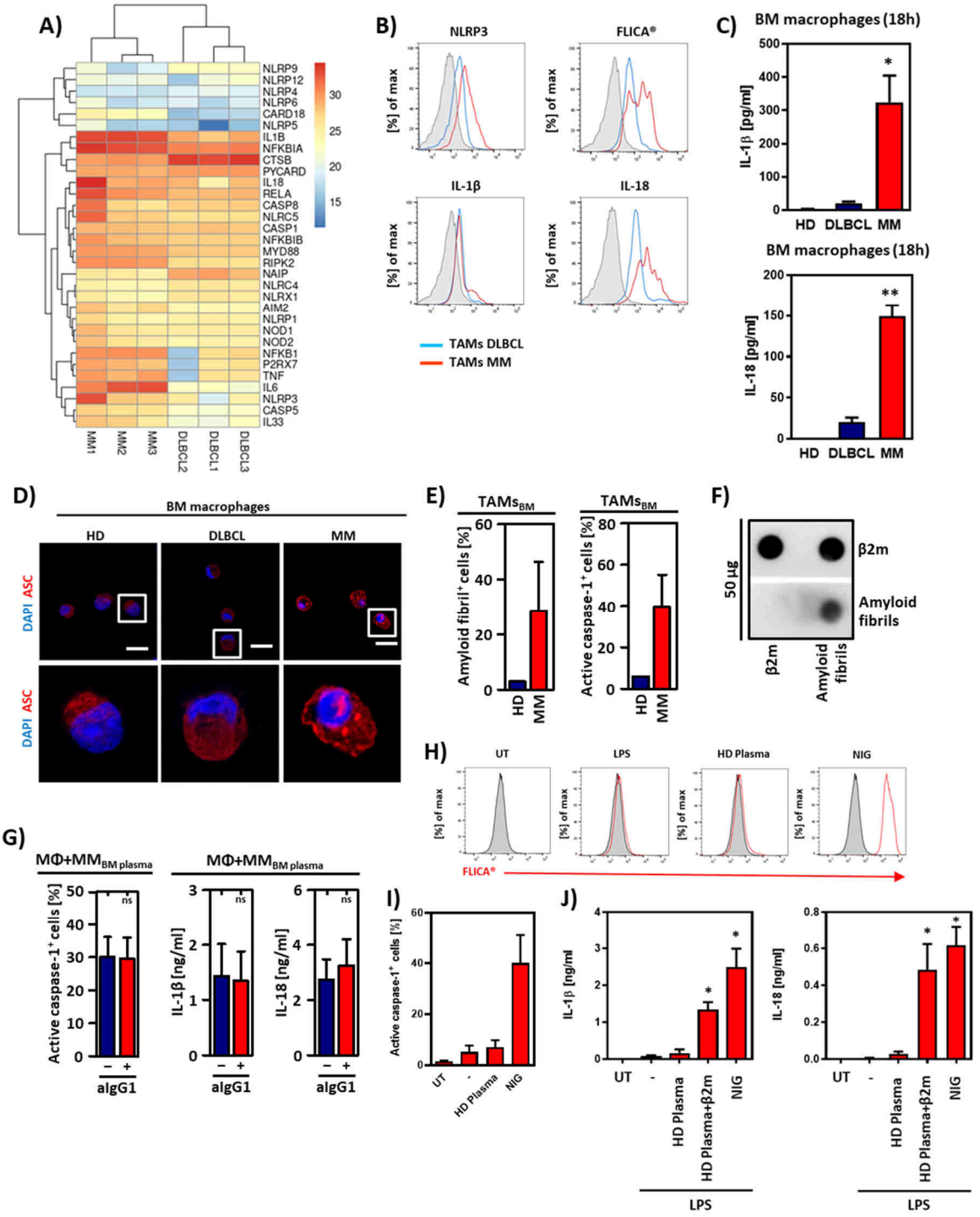

Supplementary Figure 3

Expression of inflammasome-associated markers in bone marrow (BM) macrophages, related to Figure 3. (A) CD163+/CD15- TAMs of MM (n=3) and DLBCL patients (n=3) were isolated from BM cell-aspirates by FACS-sorting (CD163+/CD15-). RNA was isolated and mRNA expression analyzed by qPCR-based arrays. The heat map compares inflammasome-related markers between BM macrophages of MM or DLBCL patients. The colors are derived from an inverted scale of housekeeping-normalized qPCR ΔCt values, with high numbers indicating high expression. **(B)** Expression of NLRP3, IL-1ß, IL-18, and caspase-1 activity (FLICA®) in isolated TAMs (blue: DLBCL; red: MM) was evaluated by FACS. The grey histograms show unstained controls. Plots are representative of three independent experiments.

(**C**) Isolated BM macrophages of healthy donors (HD) (n=3) or TAMs (DLBCL or MM, n=3) were cultivated for 18 h. Supernatants were analyzed for IL-1ß and IL-18 secretion by ELISA. (**D**) Isolated BM macrophages from healthy donors (HD) or TAMs (DLBCL or MM) were adhered on slides and stained for ASC (red). The nuclei were counter-stained with DAPI (blue). Data representative of three independent experiments are shown. (**E**) Flow cytometry using AmyTracker™ 480 and FLICA® 660 to detect percentage [%] of (left graph) amyloid fibril-positive and (right graph) active caspase-1-positive macrophages from human BM of HDs (blue bars) and TAMs from MM patients (red bars). Data representative of five different MM patients (n = 5) and three HD (n = 3) are shown. (**F**) Dot blot analysis of β2m and amyloid fibrils (total protein: 50 µg) (n = 1). (**G**) Left graph: Flow cytometry using FLICA® 660 to detect percentage [%] of active caspase-1-positive macrophages (MΦ) primed with LPS (100 ng/ml, 3 h) and overnight-co-cultured with human BM plasma of untreated MM patients (8 %) in the presence (red bar) and absence (blue bar) of an IgG1-neutralizing antibody (aIgG1) (10 µg/ml) (n = 11). Right graphs: IL-1β and IL-18 release [ng/ml] from macrophages (MΦ) primed with LPS (100 ng/ml, 3 h) and overnight-co-cultured with human BM plasma of untreated MM patients (8 %) in the presence (red bars) and absence (blue bars) of an IgG1 antibody (aIgG1) (10 µg/ml) as measured by ELISA (n = 8). (**H**) Macrophages were cultured untreated (UT), in presence of LPS (100 ng/ml, 3h), in presence of HD-derived BM plasma (8%), and of nigericin (NIG, 10µg/ml). FLICA® 660 was used to detect percentage [%] of active caspase-1-positive macrophages by flow cytometry as shown in representative FACS-histograms (**I**) and summarized for n=6 experiments. (**J**) IL-1β and IL-18 release [ng/ml] from macrophages left untreated (UT) or primed with LPS (100 ng/ml, 3 h) and treated with HD-derived BM plasma (8%) in the presence or absence of β2m (10µg/ml) as measured by ELISA (n=6). Results are expressed as mean ± SEM. *P < 0.05, **P < 0.01, ***P < 0.001. ns: not significant.

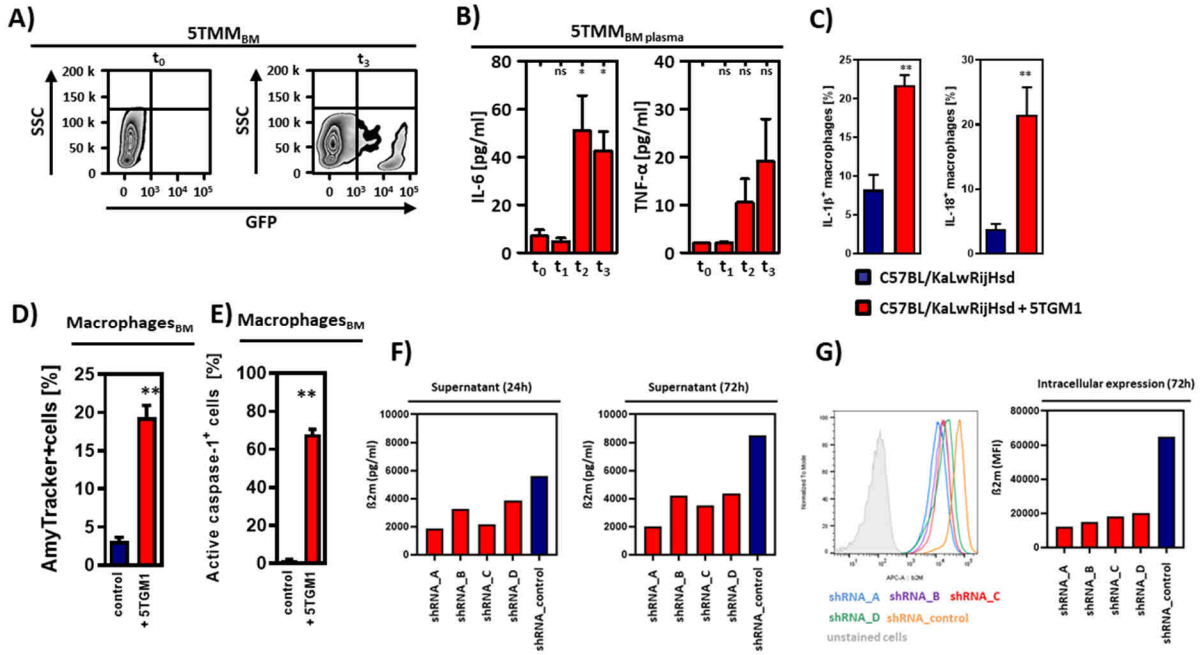

Supplementary Figure 4

Quantification of MM cells, cytokines and inflammasome activation in 5TGM1 bearing mice, related to Figure 4. (**A**) Flow cytometry to detect murine GFP-positive MM cells from BM of 5TGM1 bearing mice at different time points during MM progression (t_0, t_3). The density plots show one representative example of a total of n = 4 different. (**B**) IL-6 and TNF-α levels [pg/ml] in serum of 5TGM1 bearing mice at different time points during MM progression (t_0, t_1, t_2, t_3) as measured by LEGENDplex™ (n = 4). (**C**) Quantification of IL-1ß or IL-18 expression depicted as the frequency [%] of positive cells in BM macrophages (GR1-, F4/80+, CD115+) of C57BL/KaLwRijHsd mice (blue bars) or 5TGM1 bearing mice (red bars) by flow cytometry (n=6). (**D, E**) Flow cytometry using AmyTracker™ 480 and FLICA® 660 to detect percentage [%] of murine (**D**) amyloid fibril-positive and (**E**) active caspase-1-positive BM macrophages of C57BL/KaLwRijHsd mice (blue bars) or 5TGM1 bearing mice (red bars) (n = 3). (**F**) 5TGM1 cells were transduced with control shRNA (blue bars) or different shRNA variants against β2m (red bars). β2m secretion as measured by ELISA (**G**) or expression as measured by flow cytometry. The gray histogram indicates the unstained control (5TGM1 cells without anti-β2m-APC). Results are expressed as mean ± SEM. *P < 0.05, **P < 0.01, ***P < 0.001. ns: not significant.

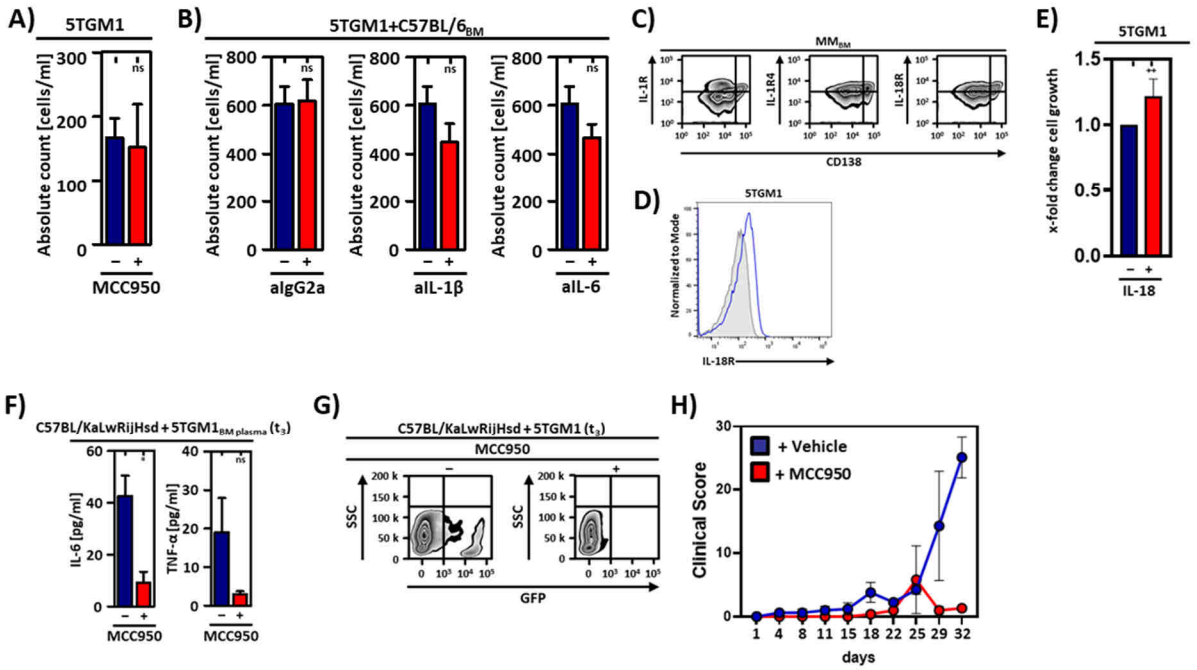

Supplementary Figure 5

Effect of MCC950 on 5TGM1 cells, related to Figure 5. (**A**) Absolute cell counts as determined by flow cytometry using 123count™ eBeads to detect growth [cells/ml] of murine 5TGM1 cells in the presence (red bar) and absence (blue bar) of NLRP3-specific inhibitor MCC950 (10 µM) (n = 8). (**B**) Absolute cell counts as determined by flow cytometry using 123count™ eBeads to detect growth [cells/ml] of murine 5TGM1 cells co-cultured with murine BM cells (1:25, 96 h) from C57BL/6 mice in the presence (red bars) and absence (blue bars) of IgG2a, IL-1β and IL-6 neutralizing antibodies (aIgG2a, aIL-1β, aIL-6) (1 µg/ml). (n = 8). (**C**) Flow cytometry to detect protein expression of IL-1R, IL-1R4 and IL-18R on the surface of human $CD138^+$ macrophages from BM of untreated MM patients. The density plots show one representative example of a total of n = 8 different MM patients. (**D**) Flow cytometry to detect protein expression of IL-18R (blue line) on the surface of 5TGM1 cells. Gray histogram indicates the isotype control. (**E**) 5TGM1 cells were stimulated with murine recombinant IL-18 (100ng/ml, 24h) and cell growth was measured by flow cytometry using 123count™ eBeads to detect growth (n = 4). (**F**) IL-6 and TNF-α levels [pg/ml] in serum of untreated (blue bars) and MCC950-treated (20 mg/kg) (red bars) mice during MM progression (t3) as measured by LEGENDplex™ (n = 4). (**G**) Flow cytometry to detect murine GFP-positive MM cells from BM of untreated and MCC950-treated (20 mg/kg) mice during MM progression (t3) (n = 4). Density plots show one representative example of 4 independent experiments. (**H**) Clinical Score of C57BL/KaLwRijHsd mice challenged with 5TGM1 cells during treatment with DMSO (blue, n=5) or MCC950 (red, n=5). Results are expressed as mean ± SEM. *P < 0.05, ns: not significant.

Observation	Score points
Body weight	
No change	0
Loss of body weight in %= score points	1 bis 20
Los of body weight >20%	20
Motility	
Spontaneous (normal behavior, social contacts)	0
Spontaneous but reduced	1
Moderately reduced activity	2
Motility only after stimulation	5
Isolation, lethargy, coordination disorders	10
Clinical complications	
Paralysis	20

Supplemental Table 2. Clinical scoring of mice, related to Figure S5.